Part V

Spatial interactions and pattern models

Turing Model II: Experimental validations: two recent examples

Week 11, 2019

Patterns in Nature

Rules

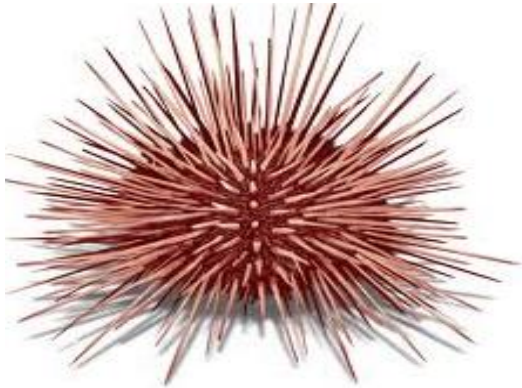

THE CHEMICAL BASIS OF MORPHOGENESIS

By A. M. TURING, F.R.S. *University of Manchester*

(*Received* 9 *November* 1951—*Revised* 15 *March* 1952)

It is suggested that a system of chemical substances, called morphogens, reacting together and diffusing through a tissue, is adequate to account for the main phenomena of morphogenesis. Such a system, although it may originally be quite homogeneous, may later develop a pattern or structure due to an instability of the homogeneous equilibrium, which is triggered off by random disturbances. Such reaction-diffusion systems are considered in some detail in the case of an isolated ring of cells, a mathematically convenient, though biologically unusual system. The investigation is chiefly concerned with the onset of instability. It is found that there are six essentially different forms which this may take. In the most interesting f
appear on the ring. It is suggested that this might account, for instance, fo
on *Hydra* and for whorled leaves. A system of reactions and diffusion on
sidered. Such a system appears to account for gastrulation. Another re
dimensions gives rise to patterns reminiscent of dappling. It is also sug
waves in two dimensions could account for the phenomena of phyllotaxis.

The purpose of this paper is to discuss a possible mechanism by which
may determine the anatomical structure of the resulting organism. The the
new hypotheses; it merely suggests that certain well-known physical laws a
for many of the facts. The full understanding of the paper requires a gooc
matics, some biology, and some elementary chemistry. Since readers can
experts in all of these subjects, a number of elementary facts are explained,
text-books, but whose omission would make the paper difficult reading.

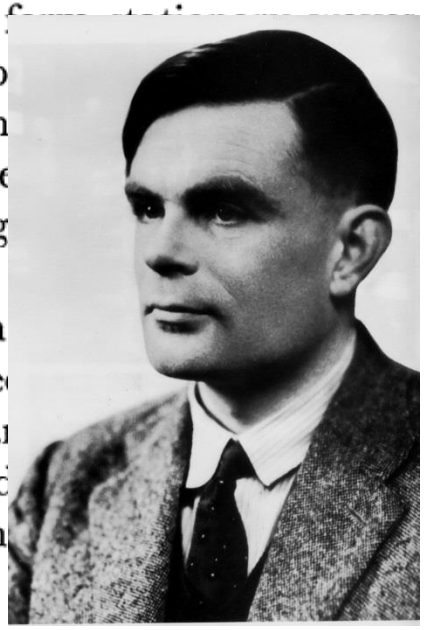

What did he discover

$$\partial_t u_1 = f_1(u_1, u_2) + D_1 \partial_x^2 u_1,$$
$$\partial_t u_2 = f_2(u_1, u_2) + D_2 \partial_x^2 u_2,$$

Generalized reaction-diffusion equations

His insights:

1. ≥2 inter…ation to occu…
2. Diffusio… influenc… …
3. Instabil… …ar wavelength
4. Diffusion coefficients of two reagents differ substantially.

However, there are 60 years between Turing published his model and some biologist actually assess this criteria!

The first experimental validation of Turing Pattern

Transition from a uniform state to hexagonal and striped Turing patterns

Q. Ouyang & Harry L. Swinney

Center for Nonlinear Dynamics and Department of Physics,
The University of Texas, Austin, Texas 78712, USA

CHEMICAL travelling waves have been studied experimentally for more than two decades[1–5], but the stationary patterns predicted by Turing[6] in 1952 were observed only recently[7–9], as patterns localized along a band in a gel reactor containing a concentration gradient in reagents. The observations are consistent with a mathematical model for their geometry of reactor[10] (see also ref. 11). Here we report the observation of extended (quasi-two-dimensional) Turing patterns and of a Turing bifurcation—a transition, as a control parameter is varied, from a spatially uniform state to a patterned state. These patterns form spontaneously in a thin disc-shaped gel in contact with a reservoir of reagents of the chlorite–iodide–malonic acid reaction[12]. Figure 1 shows examples of the hexagonal, striped and mixed patterns that can occur. Turing patterns have similarities to hydrodynamic patterns (see, for example, ref. 13), but are of particular interest because they possess an intrinsic wavelength and have a possible relationship to biological patterns[14–17].

The reaction medium is a 2.0-mm-thick polyacrylamide gel disk (25.4-mm diameter), which is sandwiched between two 0.4-mm-thick porous glass disks (Vycor glass, Corning); similar reactors have been described previously[5,18]. The gel was prepared by the procedure in ref. 7. The gel and glass disks are transparent; the pattern can therefore be detected optically. The during the redox reaction. No starch is present in the porous glass; thus concentration changes in the glass disks are not visible. The pattern is monitored in transmitted light (580 nm) with a video camera.

Beyond critical values of the control parameters (chemical concentrations and temperature), patterns emerge spontaneously from an initially uniform background. Initially, after the parameters are switched into a regime where patterns arise,

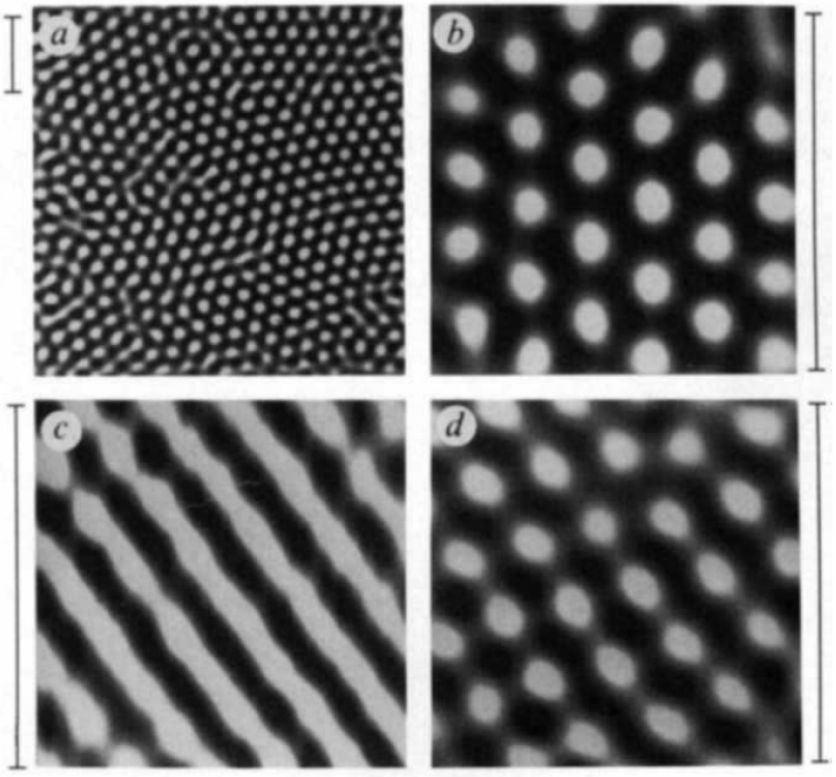

Possible networks of protein ligands may give rise to Turing patterns in the embryo.
(Kondo 2010)

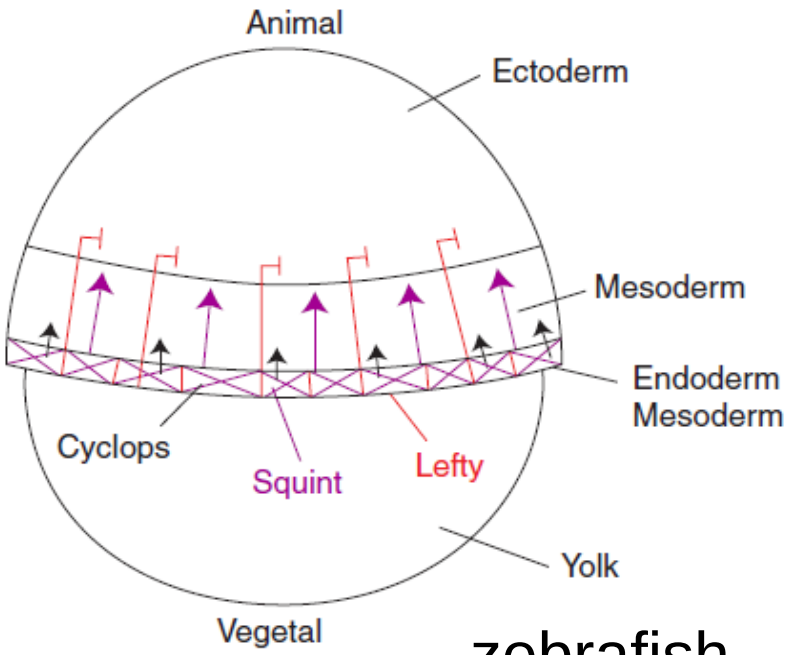

zebrafish

Figure 2. Mesoderm and endoderm induction in zebrafish. Ectoderm, mesoderm, and mesendoderm

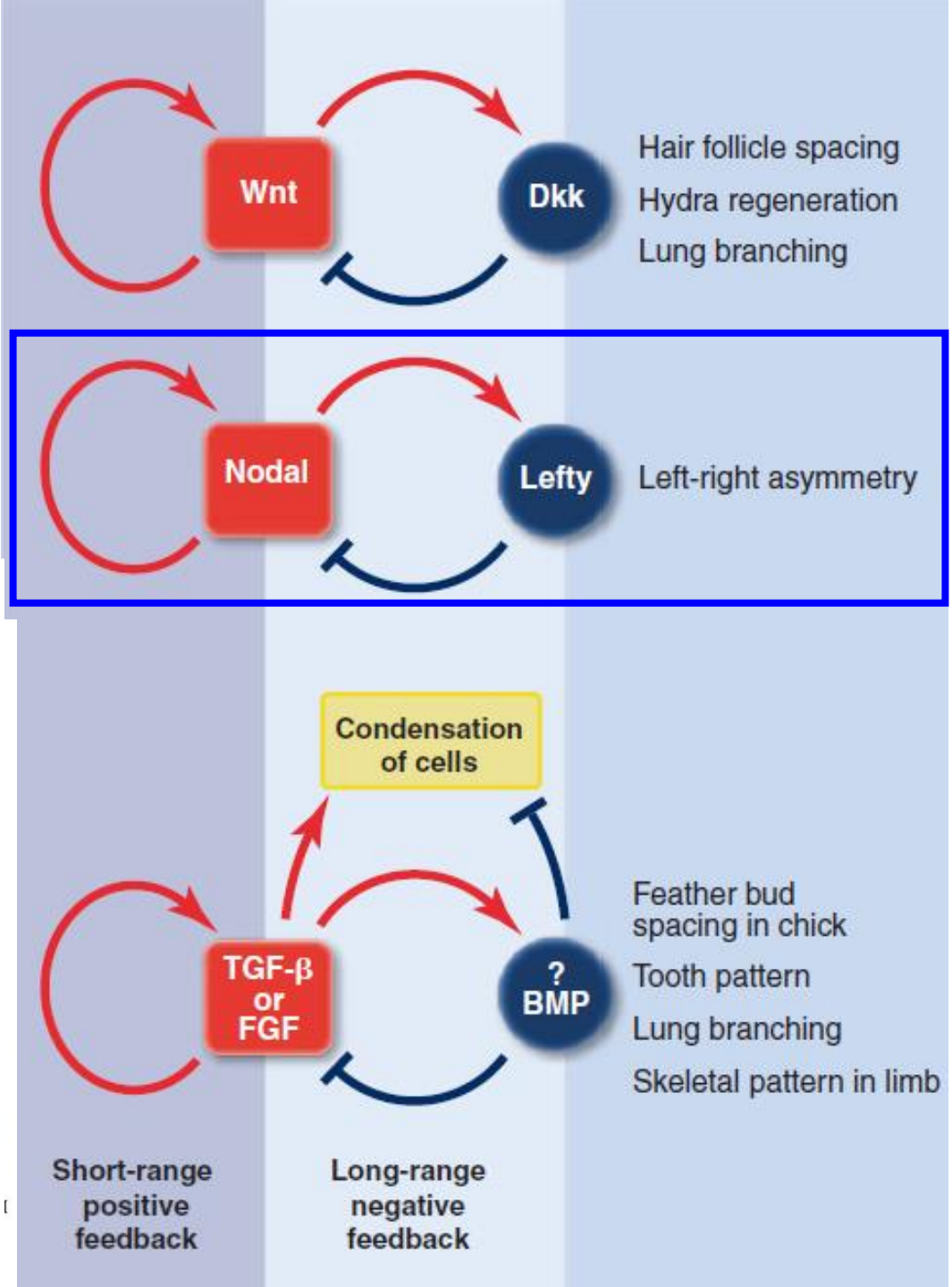

Study I:
the direct experimental evidence

Science
AAAS

Differential Diffusivity of Nodal and Lefty Underlies a Reaction-Diffusion Patterning System

Patrick Müller *et al.*

Science **336**, 721 (2012);
DOI: 10.1126/science.1221920

Biophysics of signal movements

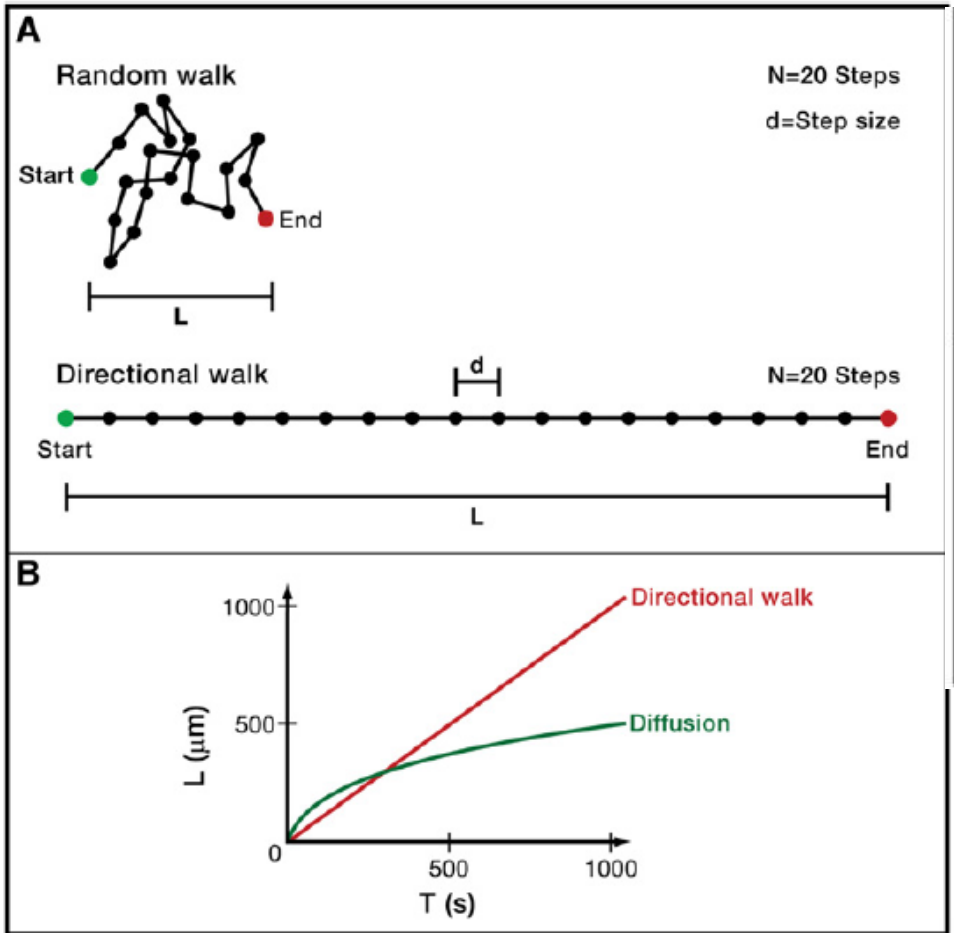

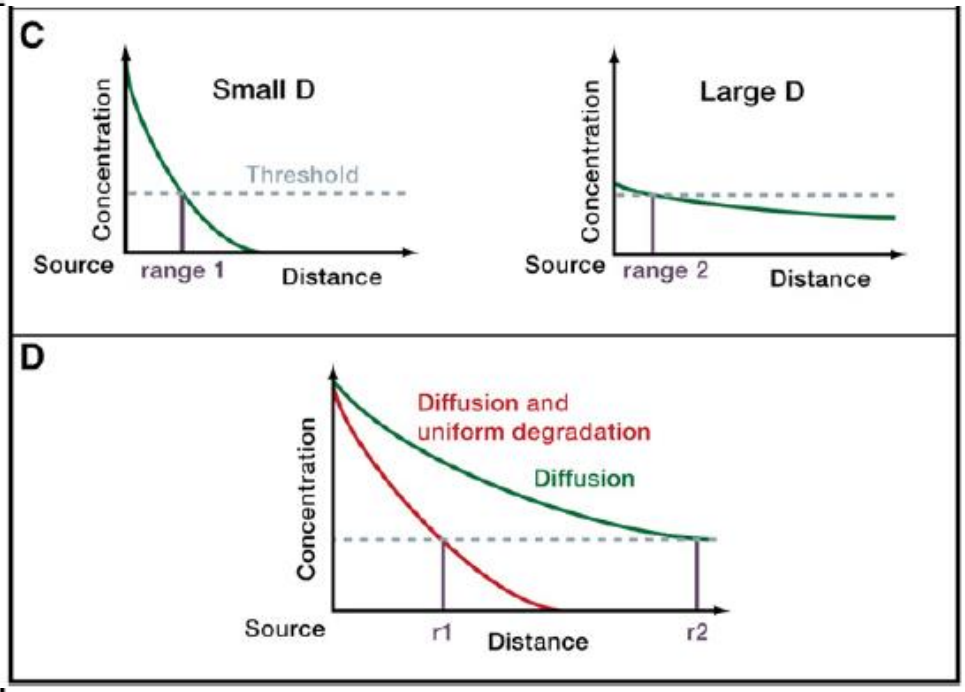

Counter arguments

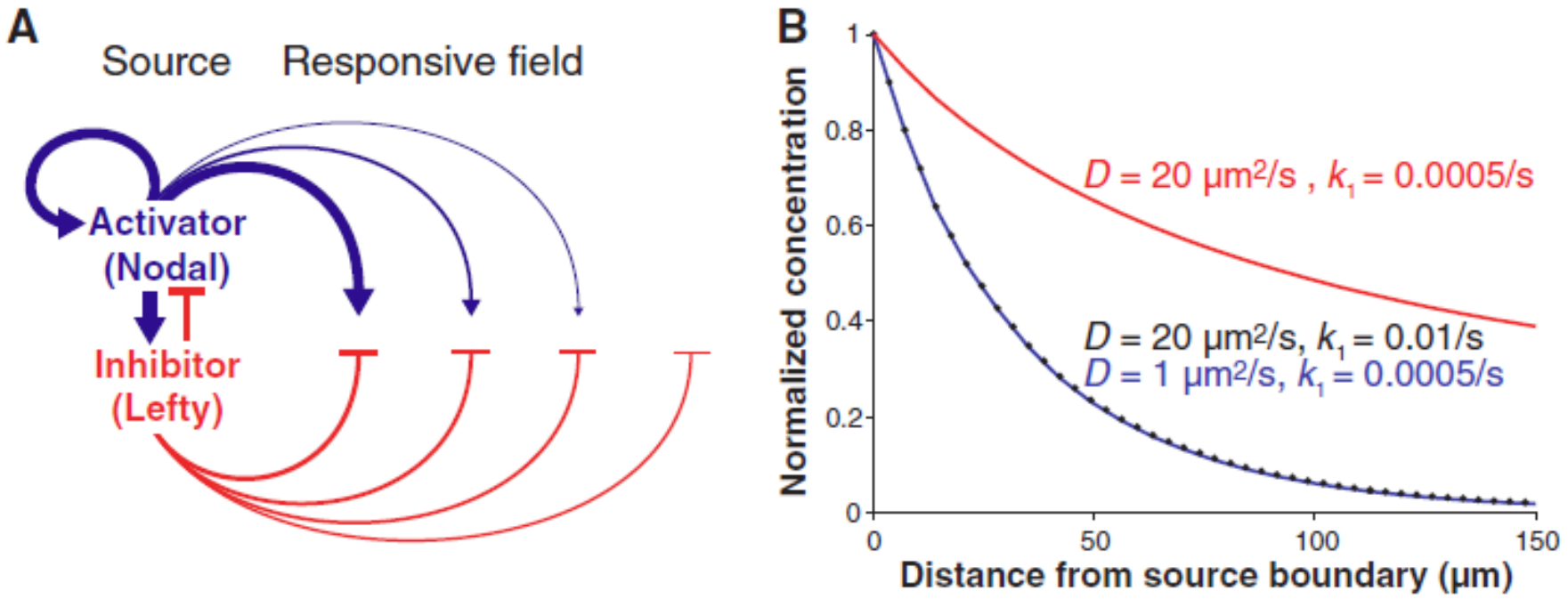

Fig. 1. Model of the Nodal/Lefty activator/inhibitor reaction-diffusion system and regulation of range. (**A**) In the source, Nodal signals (blue) activate their own expression as well as the expression of Lefty (red), which inhibits Nodal production. Nodal signaling in the responsive field is inhibited by the long-range inhibitor Lefty. (**B**) Distribution is controlled by both diffusivity, D, and clearance, k_1. Highly mobile molecules that are rapidly cleared from the extracellular space (black circles) can form gradients similar to those formed by poorly diffusive molecules that are slowly cleared (blue). Decreasing the clearance of the more diffusive species results in a long-range gradient (red). Simulations were performed as described in text S7.

Summary prior to this study

- Nodals are short (cyclops) to mid-range (squint) activators that enhance their own expressions. The range is based on the expression distribution.
- Leftys (lefty1 and lefty2) are long range inhibitors that are activated by Nodals.
- The range could be caused by different diffusion coeffients or different clearance (degradation etc).
- The central tenet of Turning model: different diffusivty of activator and inhibitor remains to be demonstrated *in vivo*.

This study performed quantitative measurements of Nodal and Lefty:

- distribution
- clearance
- diffusivity

During zebrafish embryogenesis

Assess of fusion proteins

- To visualize Nodal and Lefty protein in vivo, the generated active fusion of fluorescent proteins (GFP and Dendra2) with cyclops, Squint, Lefty1 and Lefty2
- They must confirm the functions of these fusion proteins

To validate the function of fusion proteins

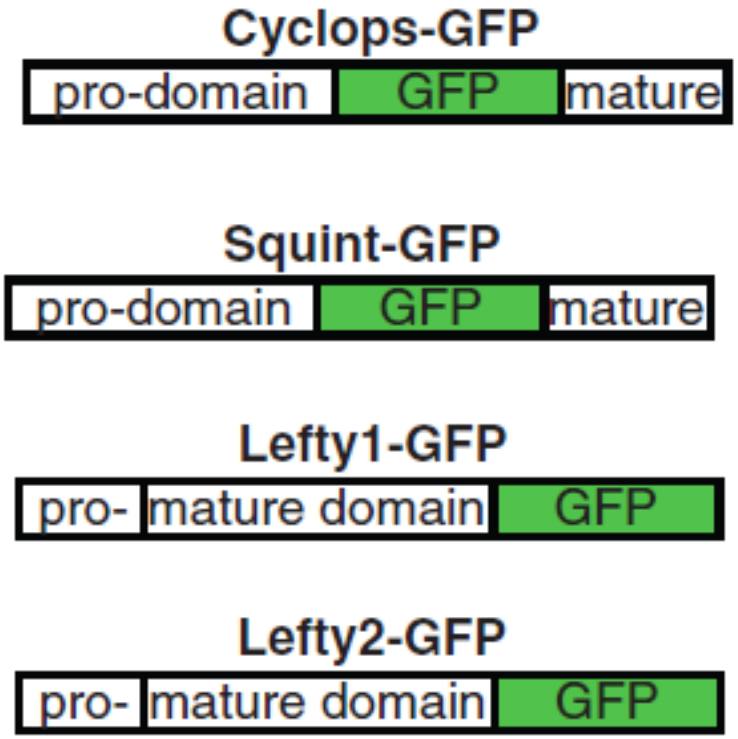

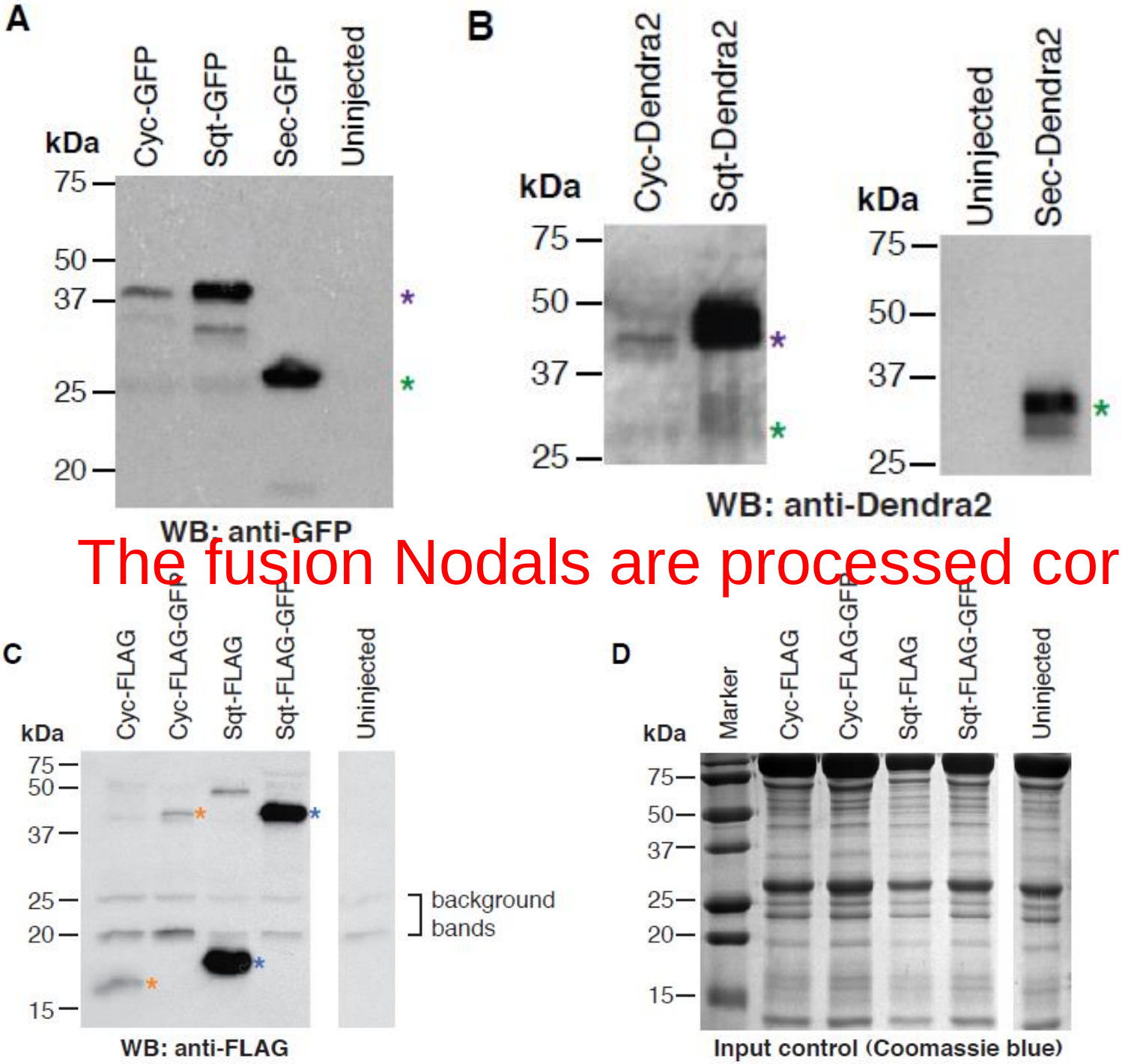
A
kDa
Cyc-GFP
Sqt-GFP
Sec-GFP
Uninjected
75
50
37
25
20
WB: anti-GFP
B
kDa
Cyc-Dendra2
Sqt-Dendra2
Uninjected
Sec-Dendra2
WB: anti-Dendra2
The fusion Nodals are processed correctly
C
kDa
Cyc-FLAG
Cyc-FLAG-GFP
Sqt-FLAG
Sqt-FLAG-GFP
Uninjected
background bands
WB: anti-FLAG
D
kDa
Marker
Cyc-FLAG
Cyc-FLAG-GFP
Sqt-FLAG
Sqt-FLAG-GFP
Uninjected
Input control (Coomassie blue)

Fusion Nodals activate downstream target similar to wt genes

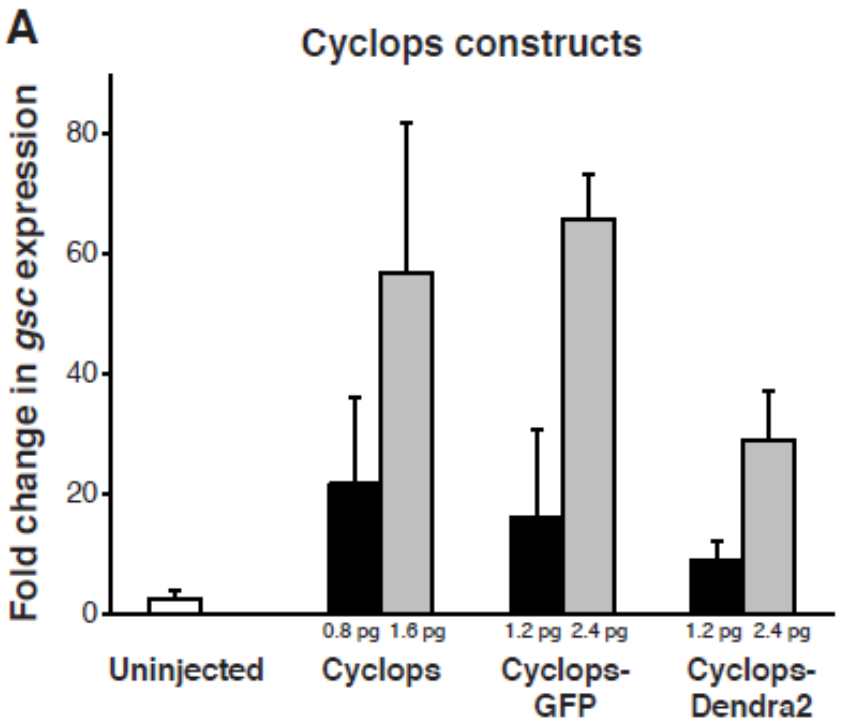

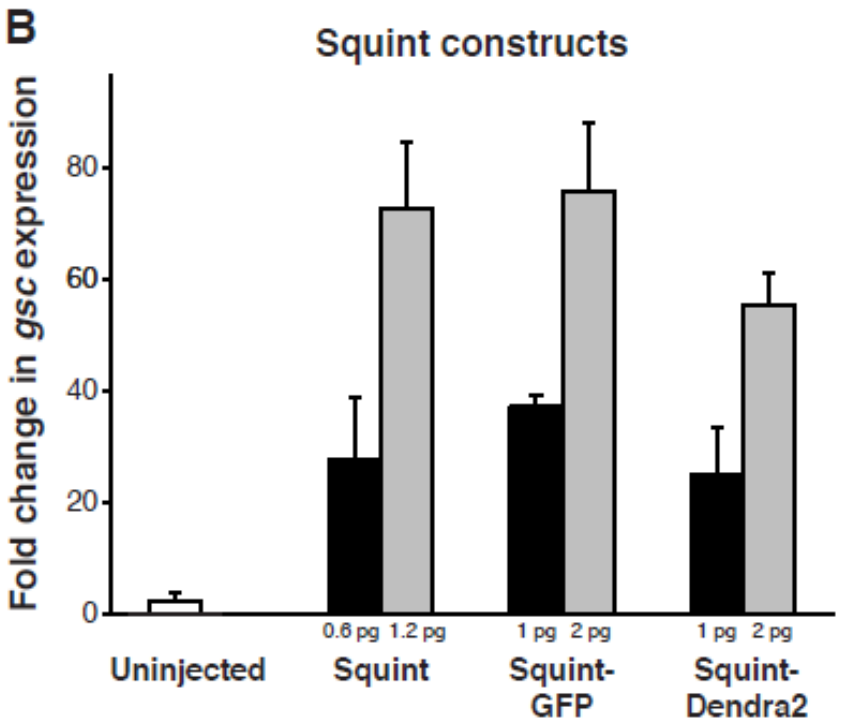

Fusion Nodals activate downstream target with similar spatial distribution to wt genes

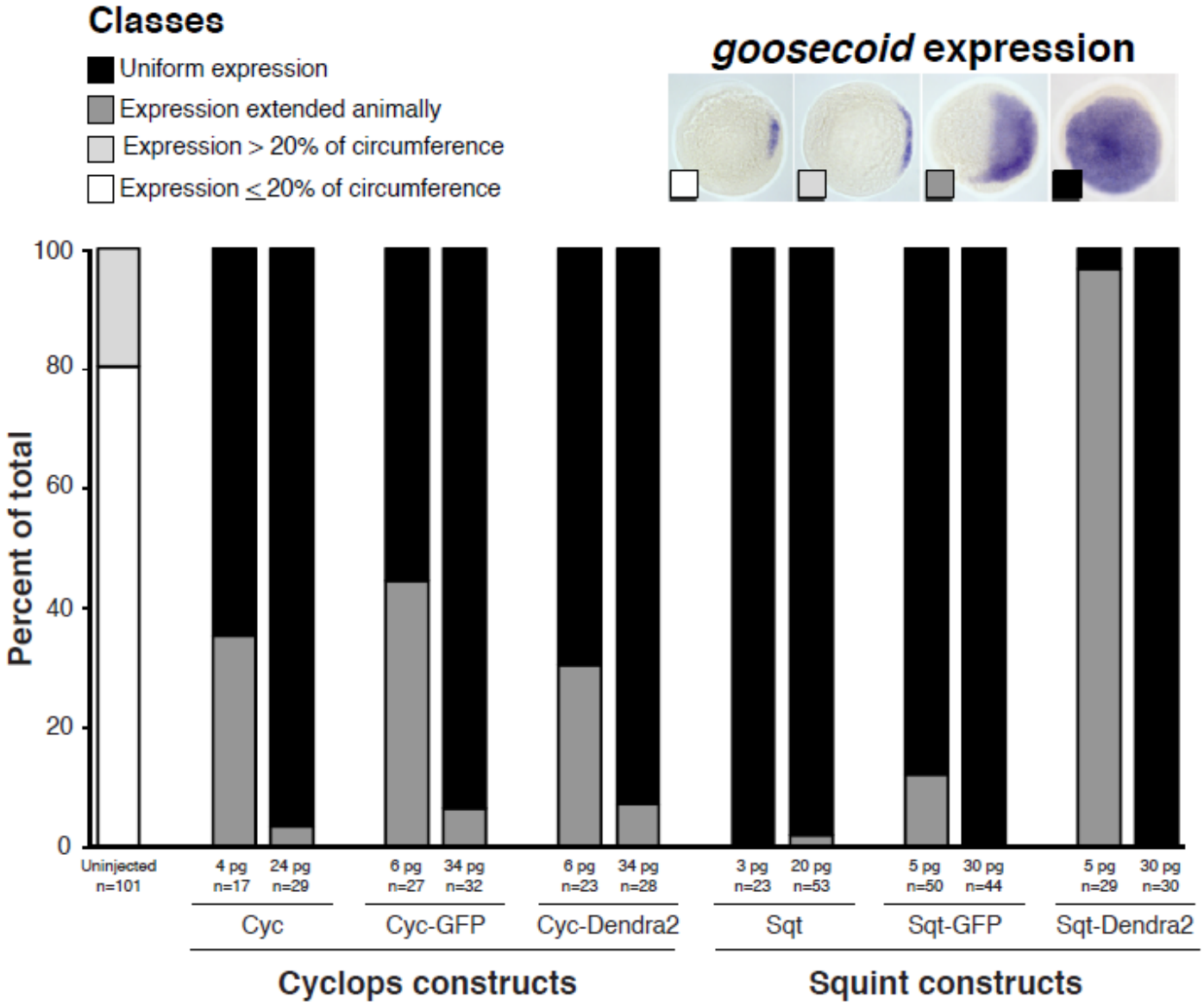

Fusion didn't change the active range of Nodals

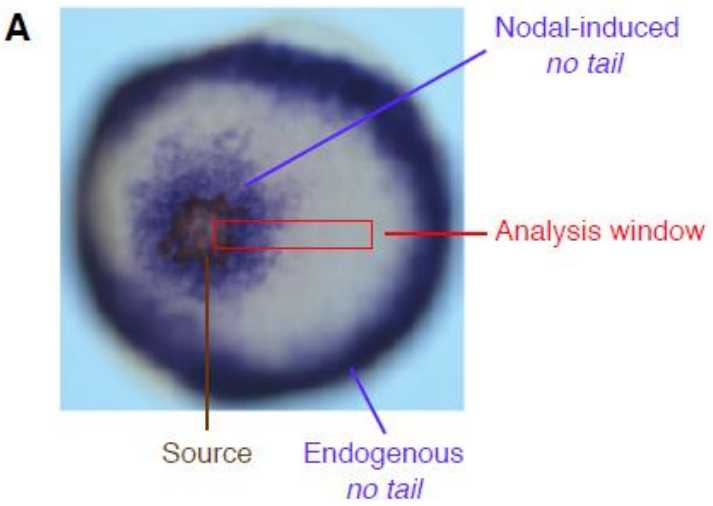

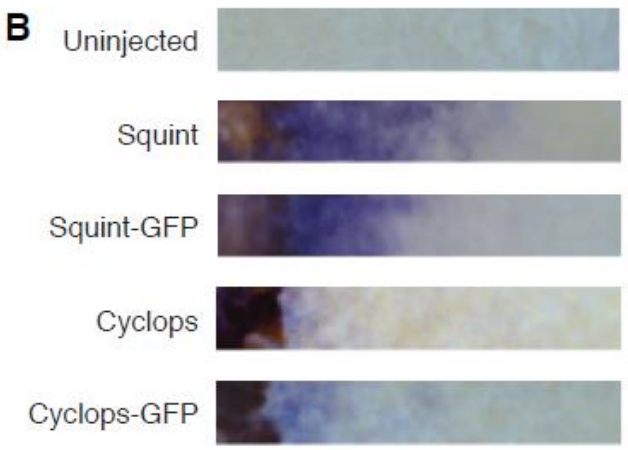

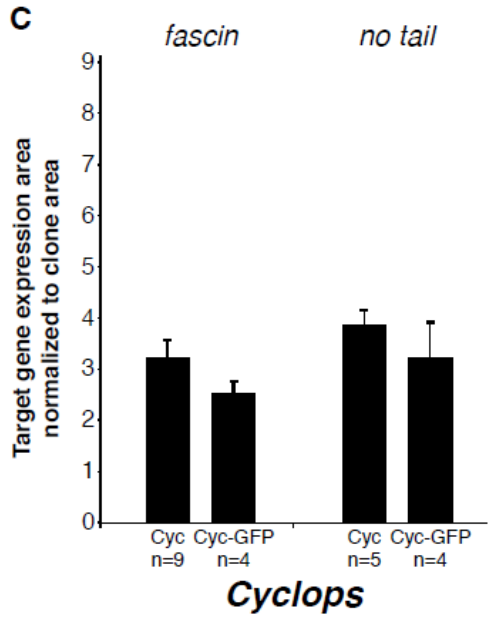

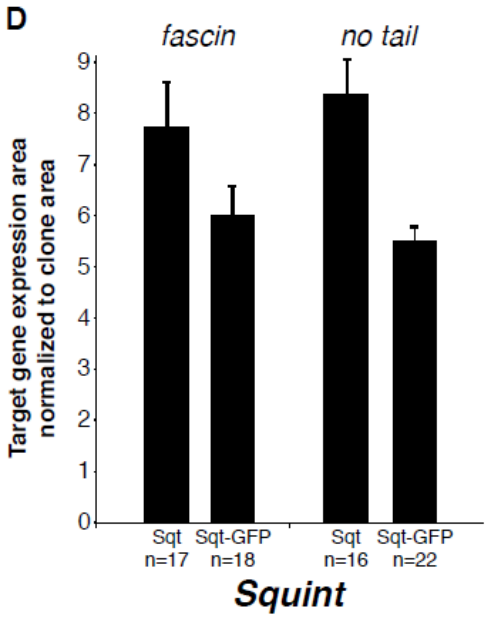

The fusion Leftys are processed correctly

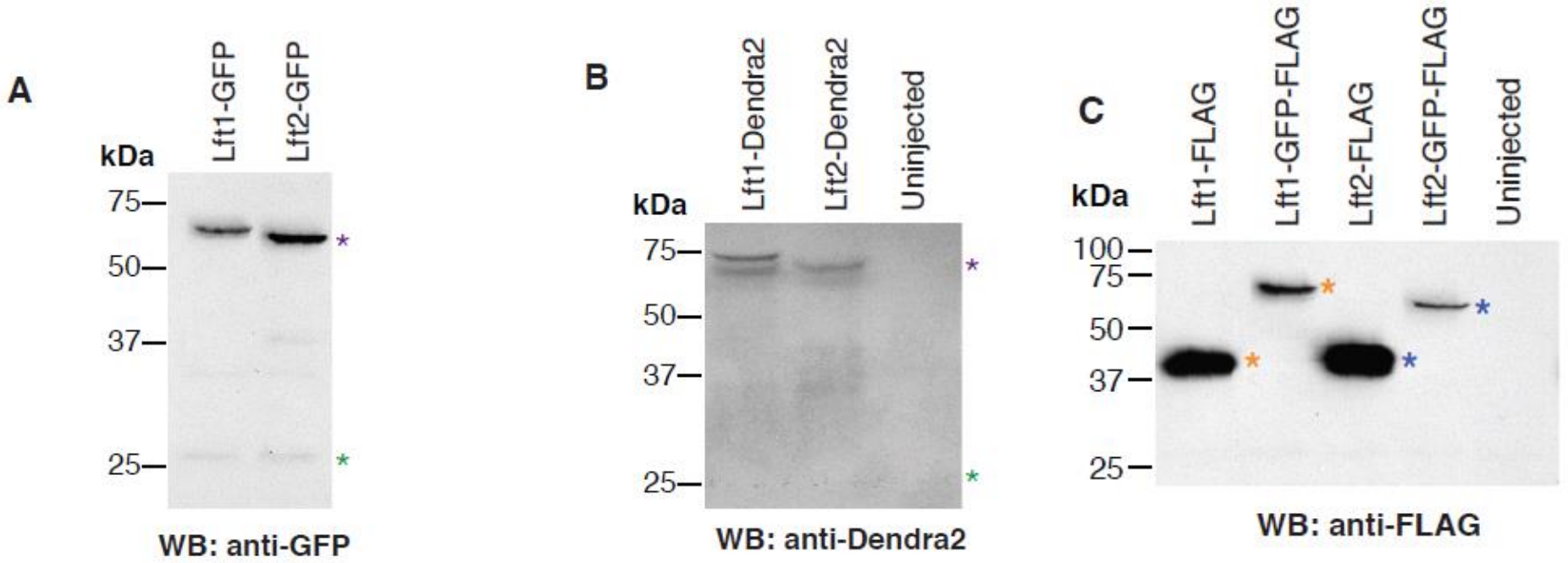

Overexpression of fusion Leftys has similar phenotypes as Nodal mutant

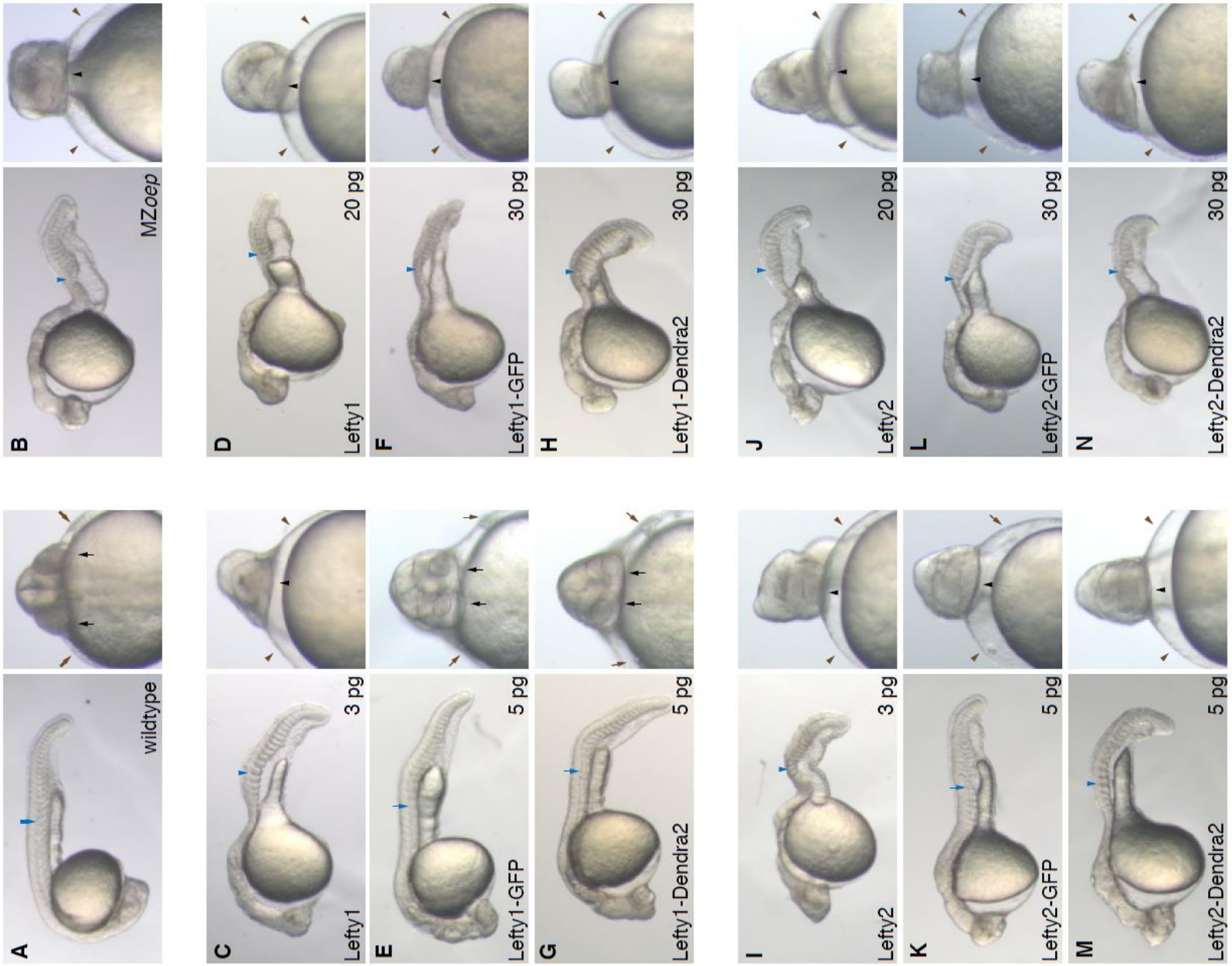

Lefty fusions inhibit Nodal targets gene similar to Lefty

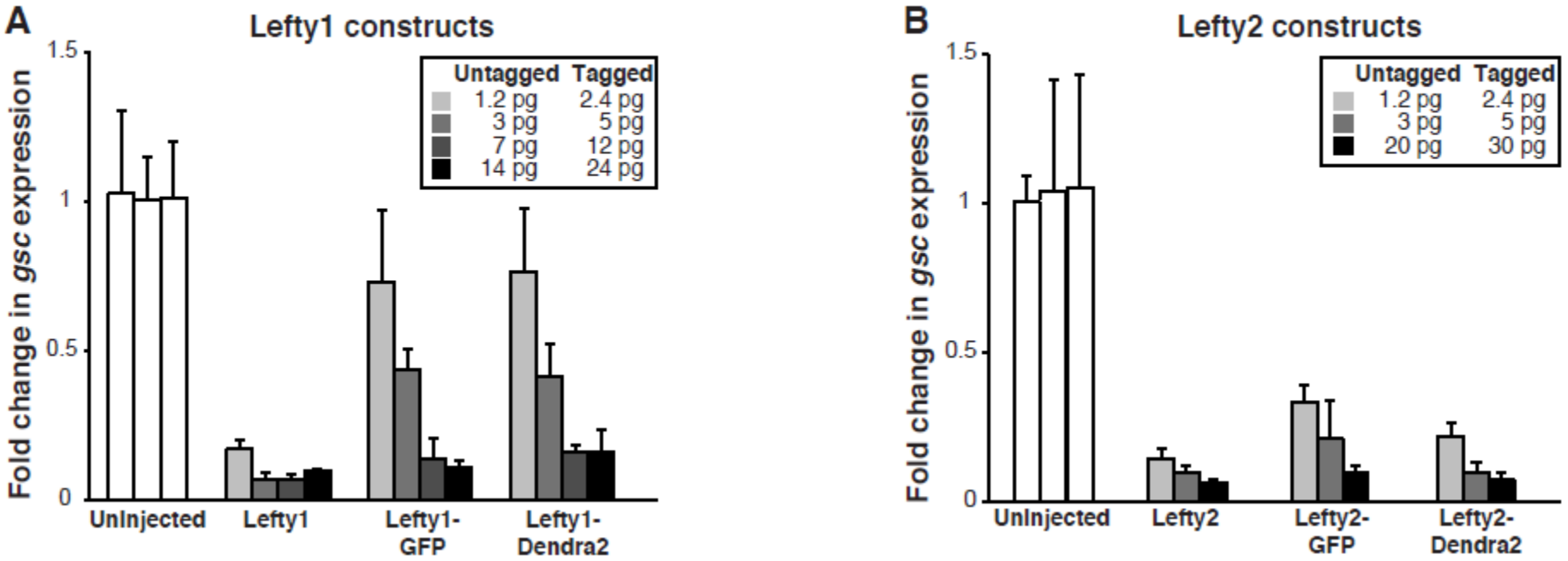

Fusion Leftys inhibit downstream target with similar spatial distribution to wt genes

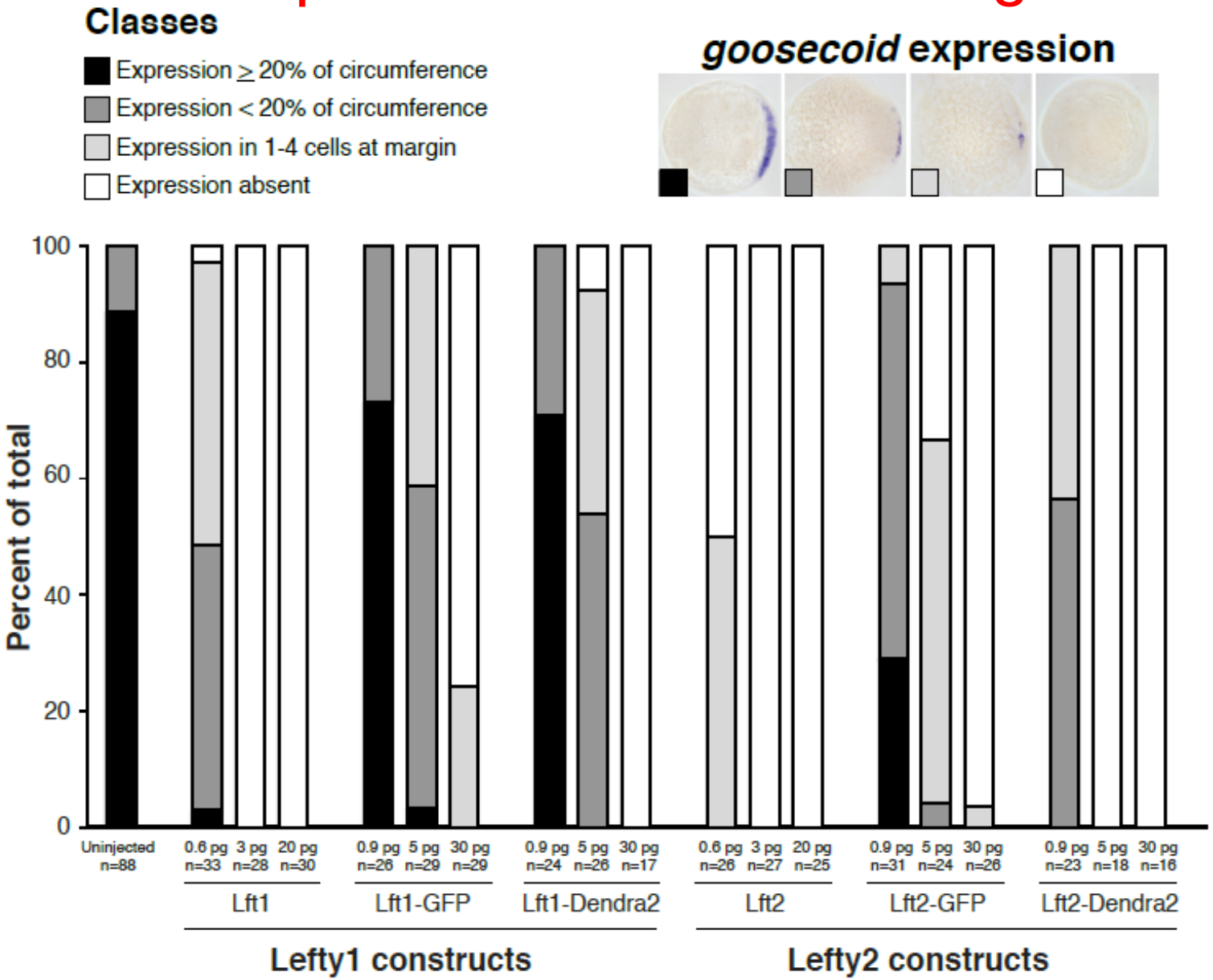

Fusion didn't change the active range of Leftys

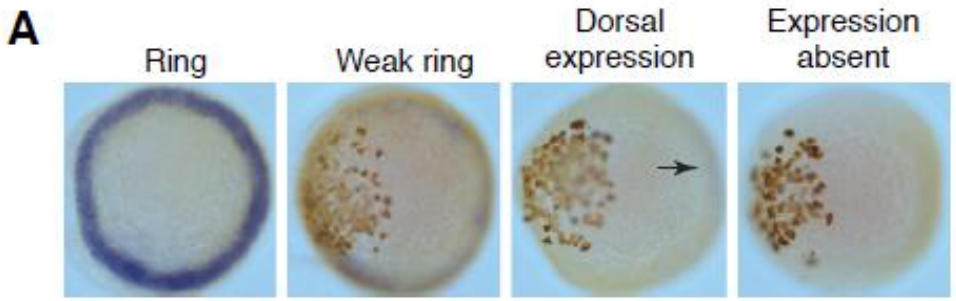

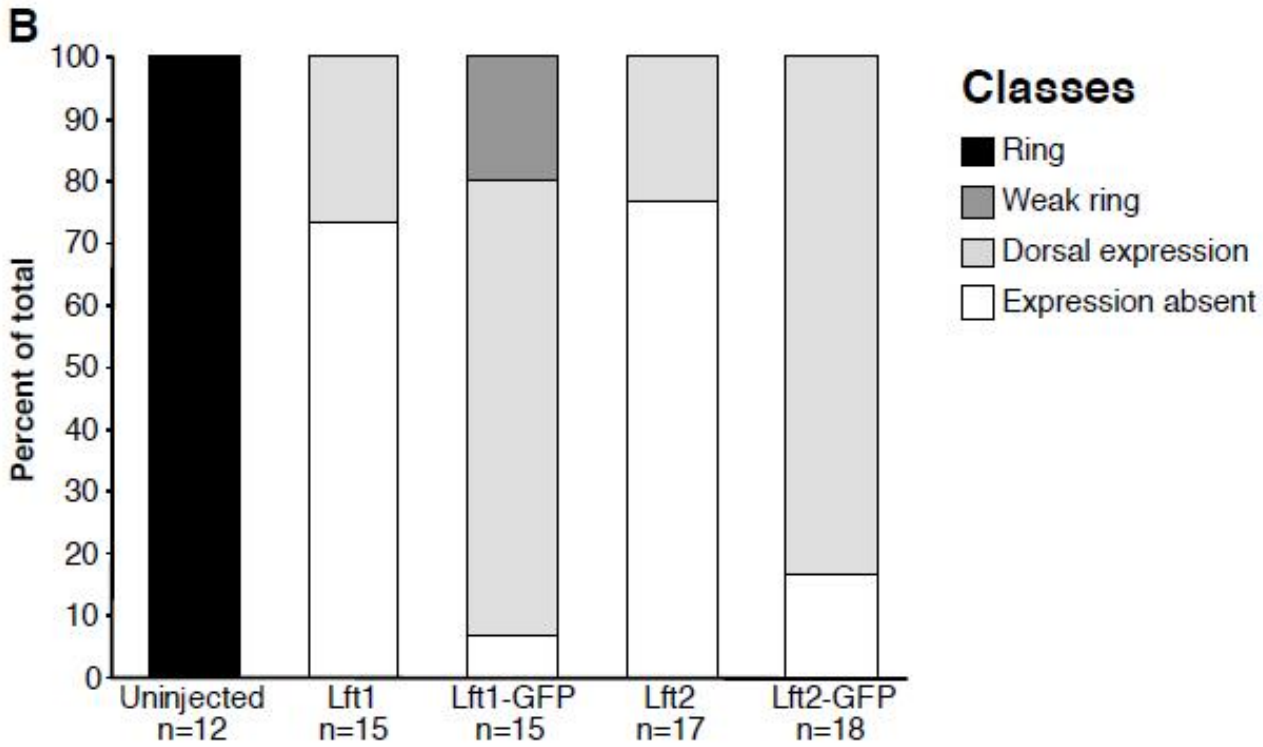

Nodals are significantly membrane-associated
Leftys are exclusively extracellular

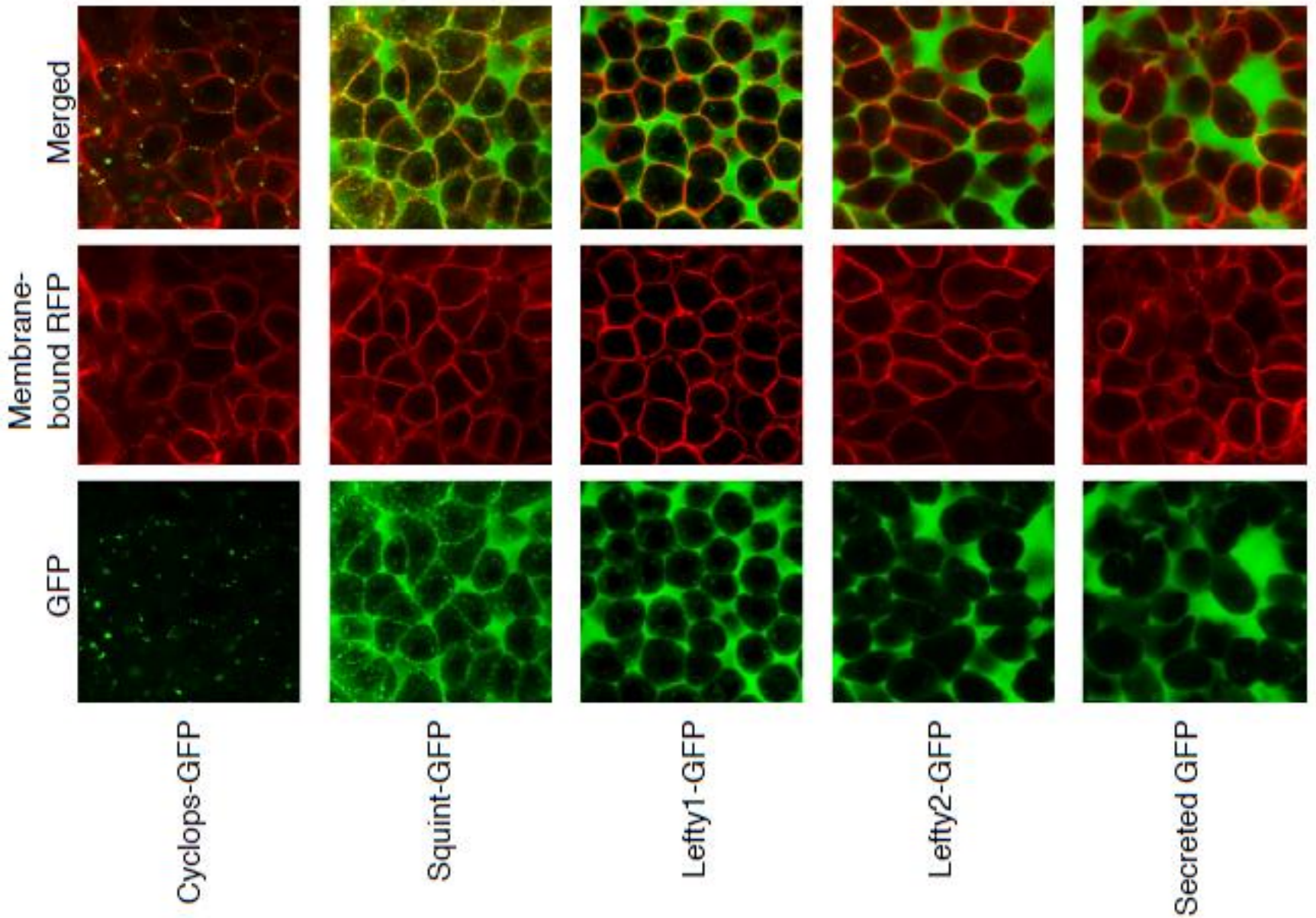

Test I: distributions: range

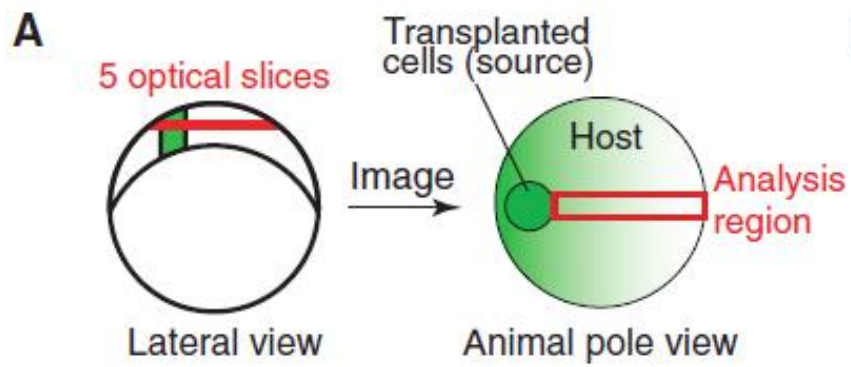

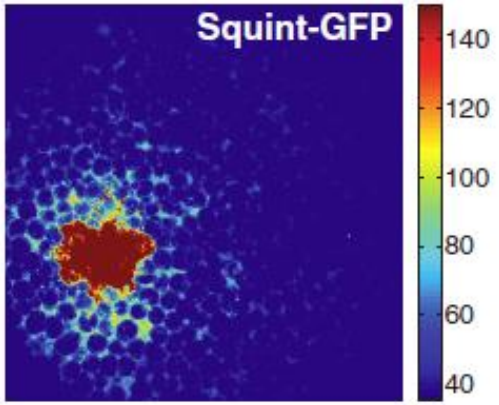

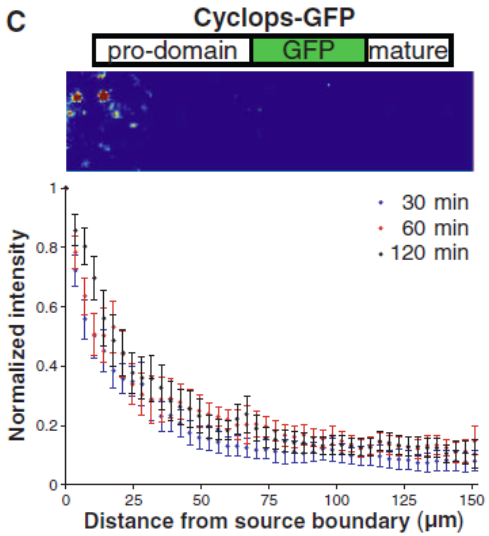

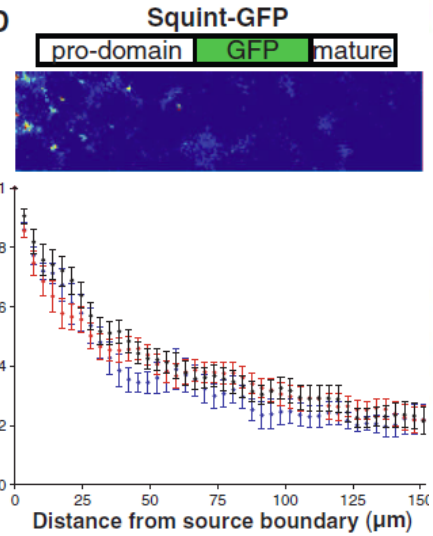

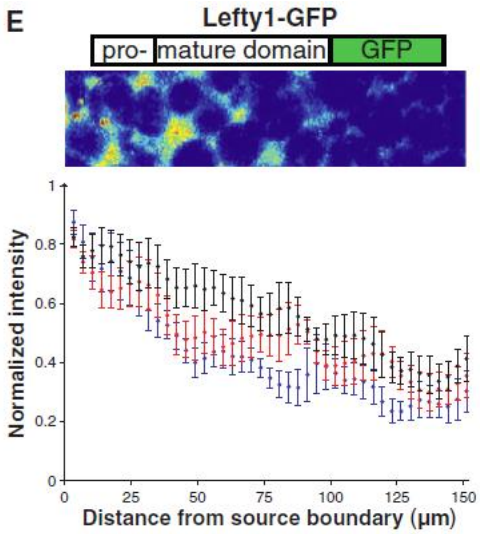

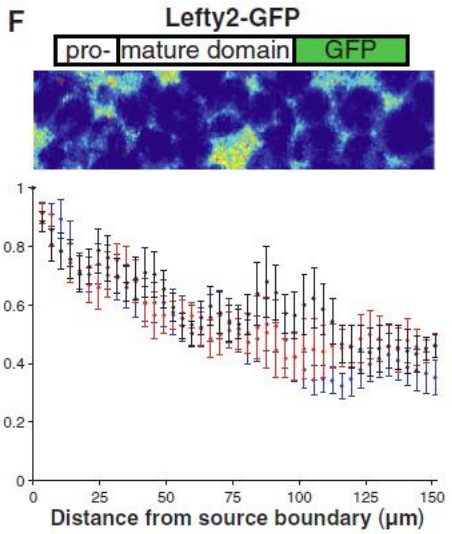

Range:

Cyclops < Squint < Lefty1 ≈ Lefty2

Test II: clearance rate

- Nodals and Leftys are constantly produced by embryo.
- How can we determine the clearance rate?
- Remember the pulse-chase assay?
- If we can just see the proteins produced at the short period of time….
- Dendra2 is the fluorescent protein to help

Dendra2

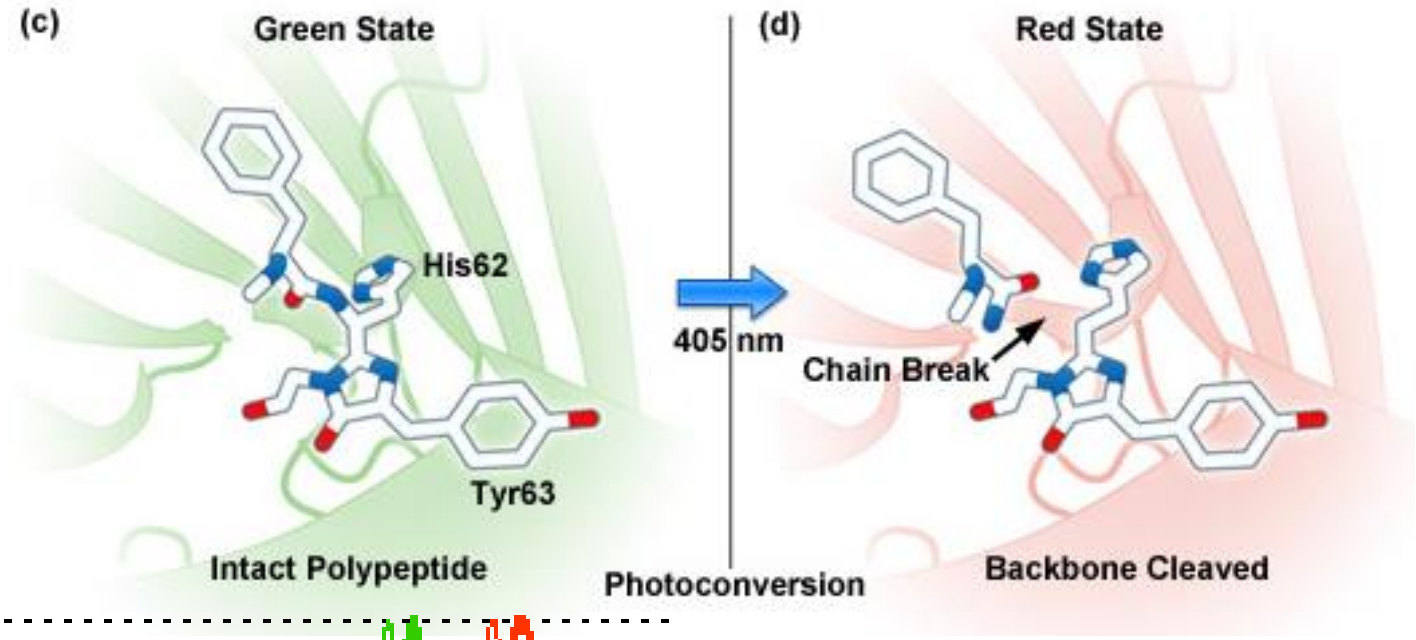

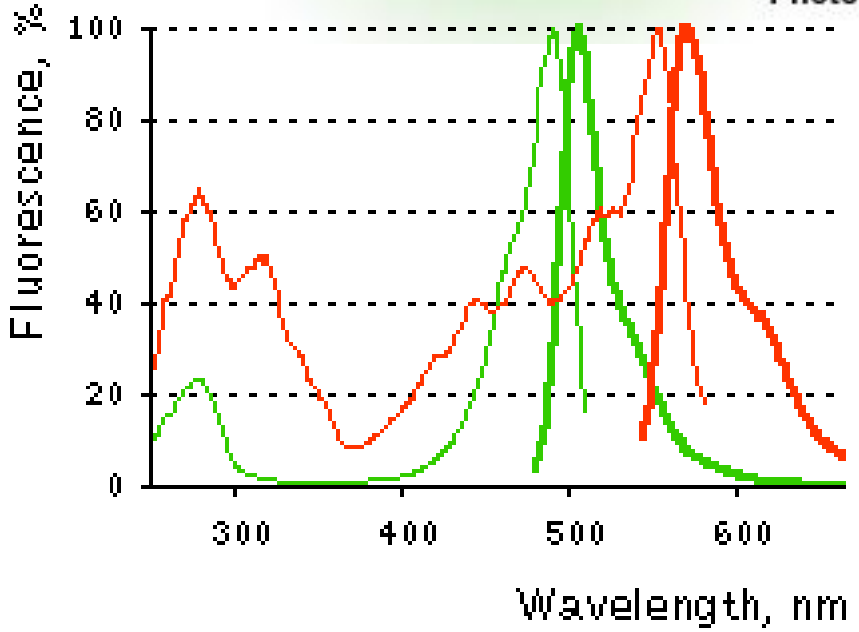

Imaging red fluorescence: tracing the spatial-temporal dynamics Nodals and Leftys produced in a short period of time.

Test II: clearance rate

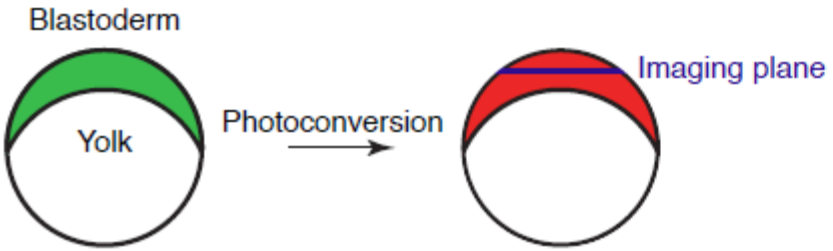

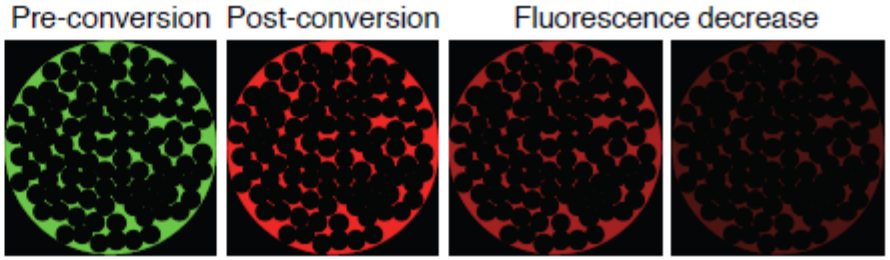

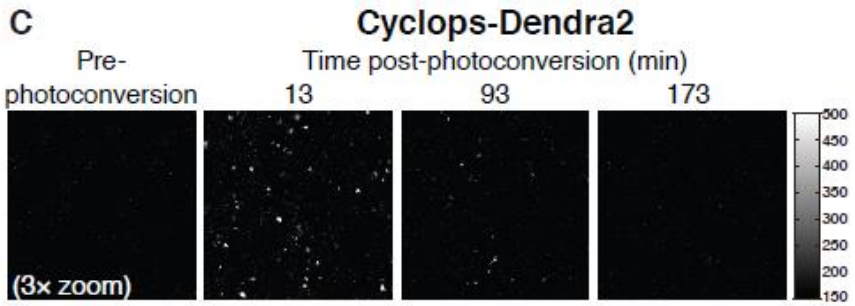

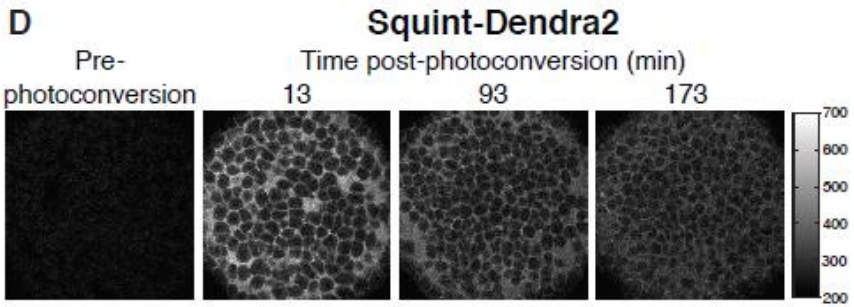

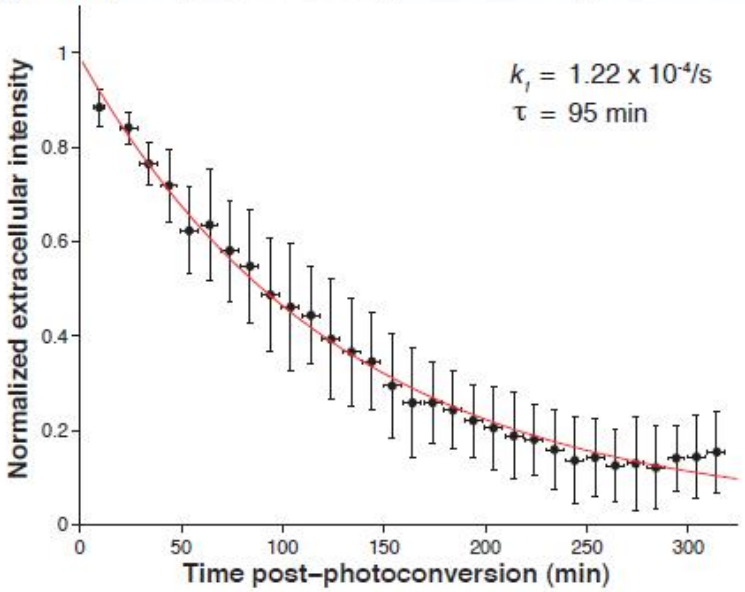

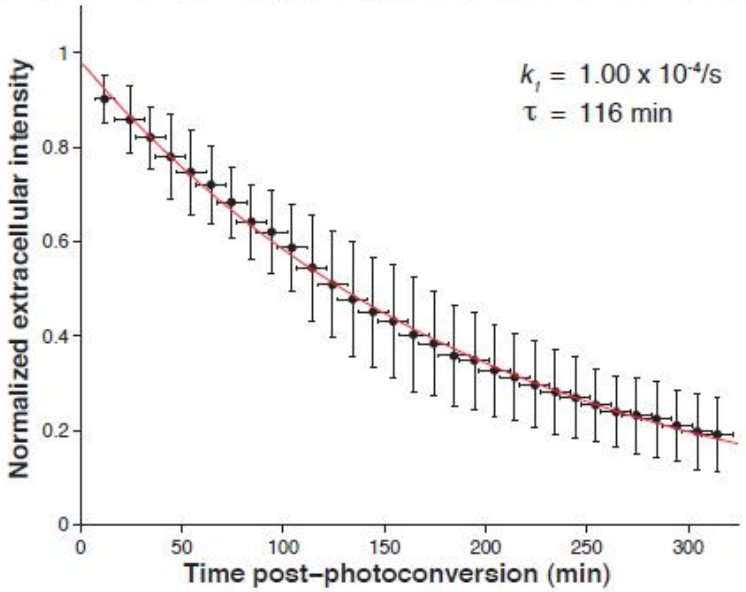

Measure only extracellular diffusion?

Intracellular fluorescence dye

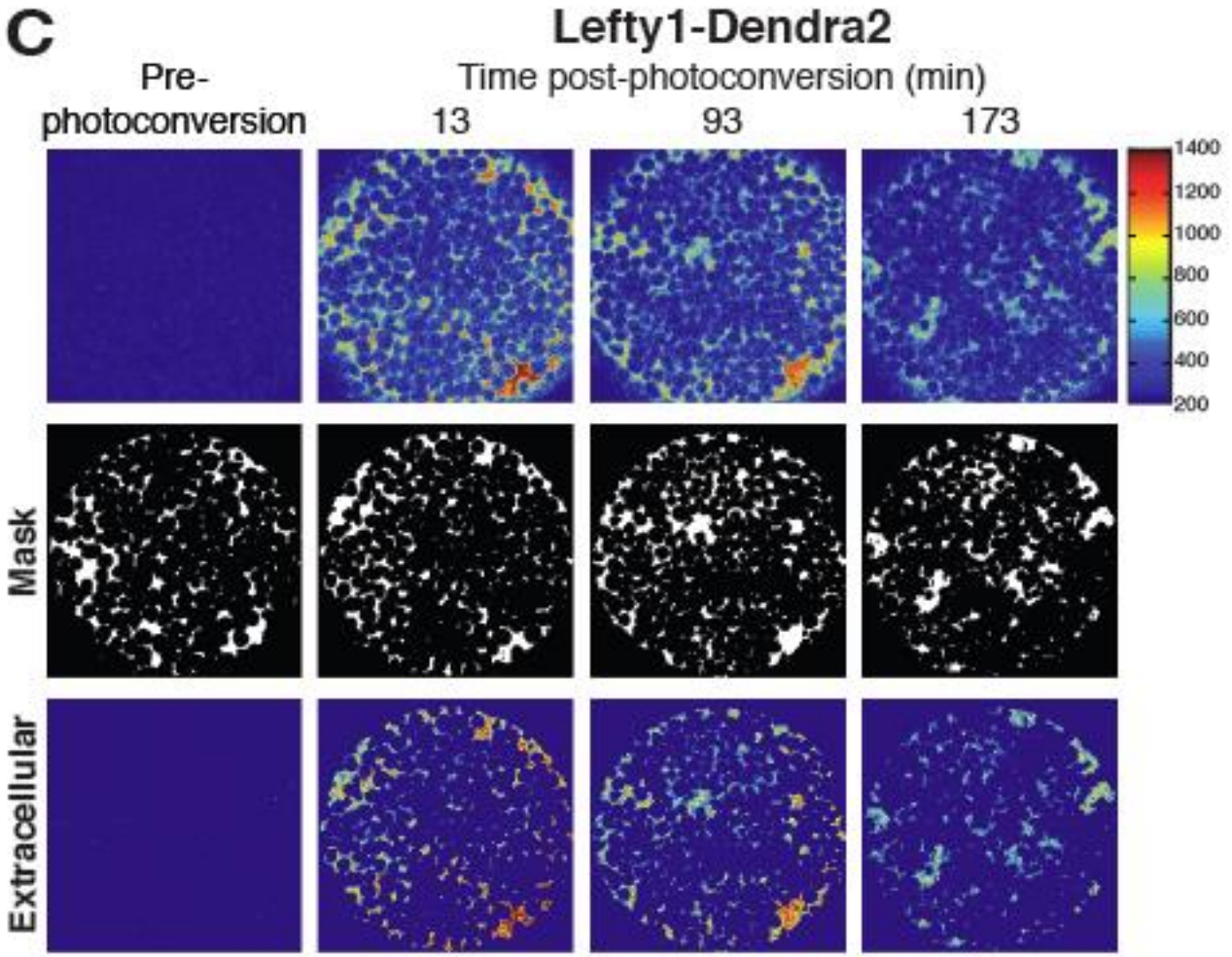

Test II: clearance rate (cont.)

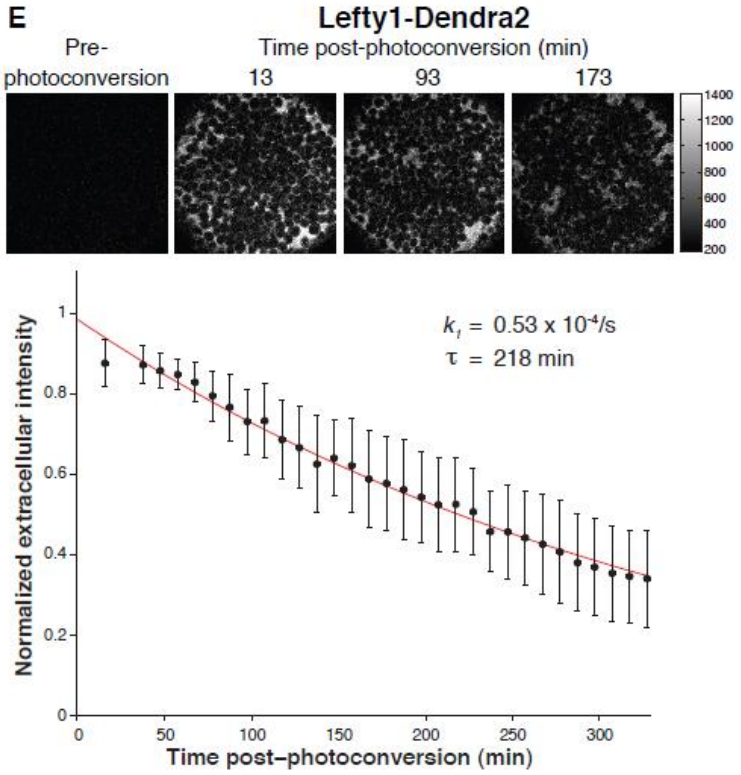

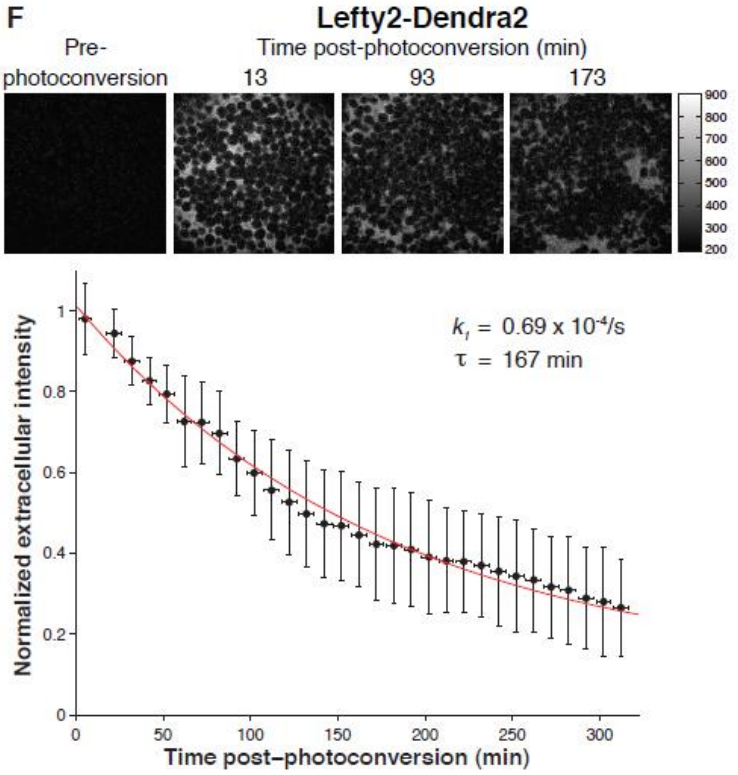

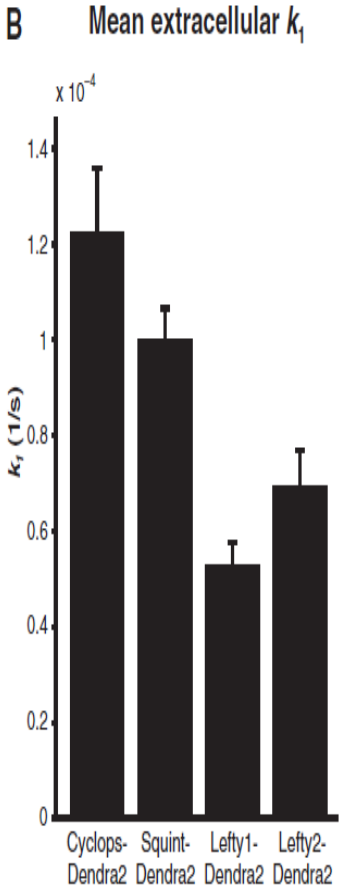

The clearance rates are faster with Nodals, but the difference is too small to explain the distribution data.

Test III: diffusion coefficient in vivo

- Is diffusion underlies the large difference in activator (Nodals) and inhibitor (Leftys) distribution?
- The technologies has been developed more than 15 years ago!
- Fluorescent recovery after photobleaching (FRAP) is the most widely used methods and supported by all the modern point-scanning laser confocal microscopy.

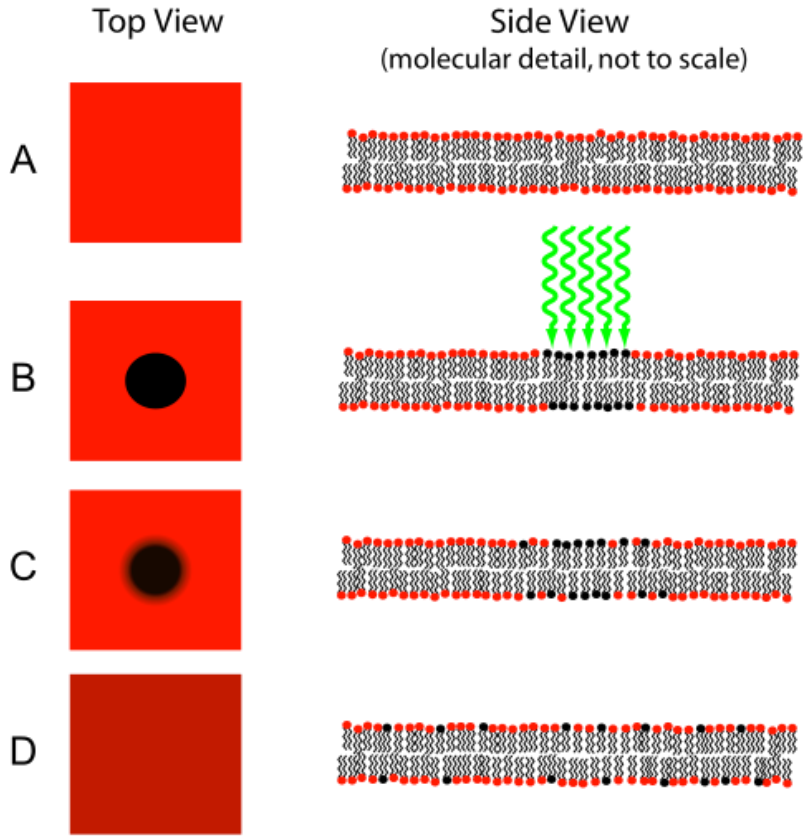

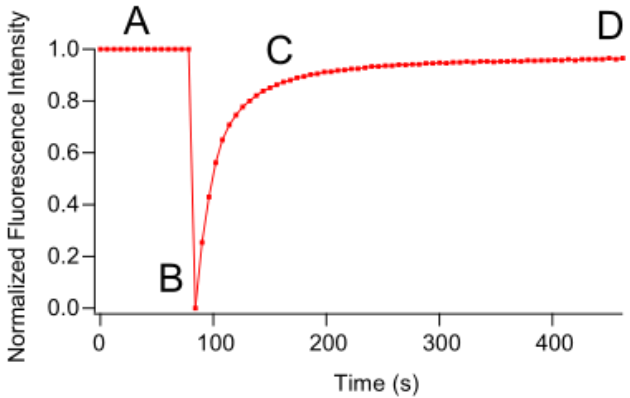

Test III: diffusion coefficient in vivo

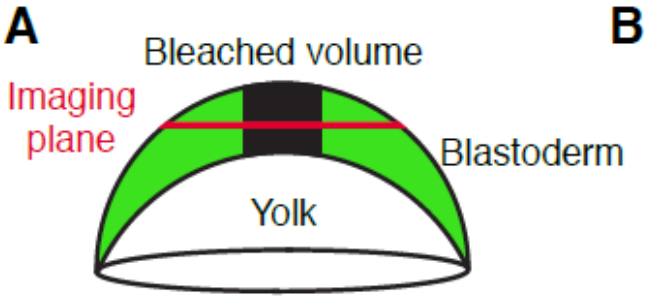

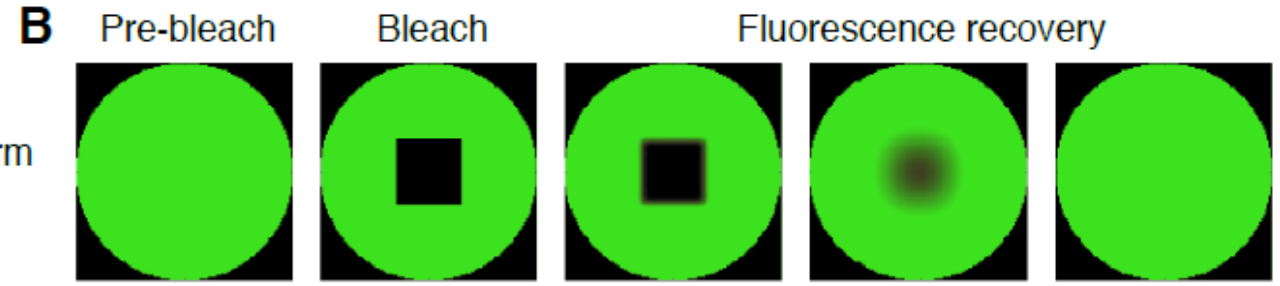

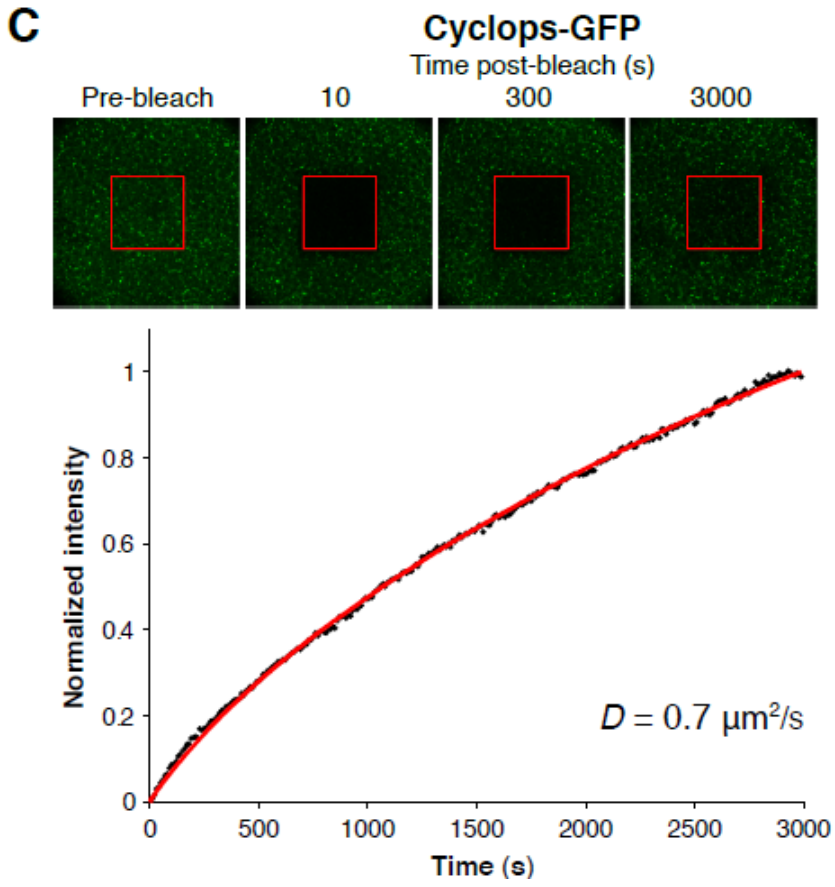

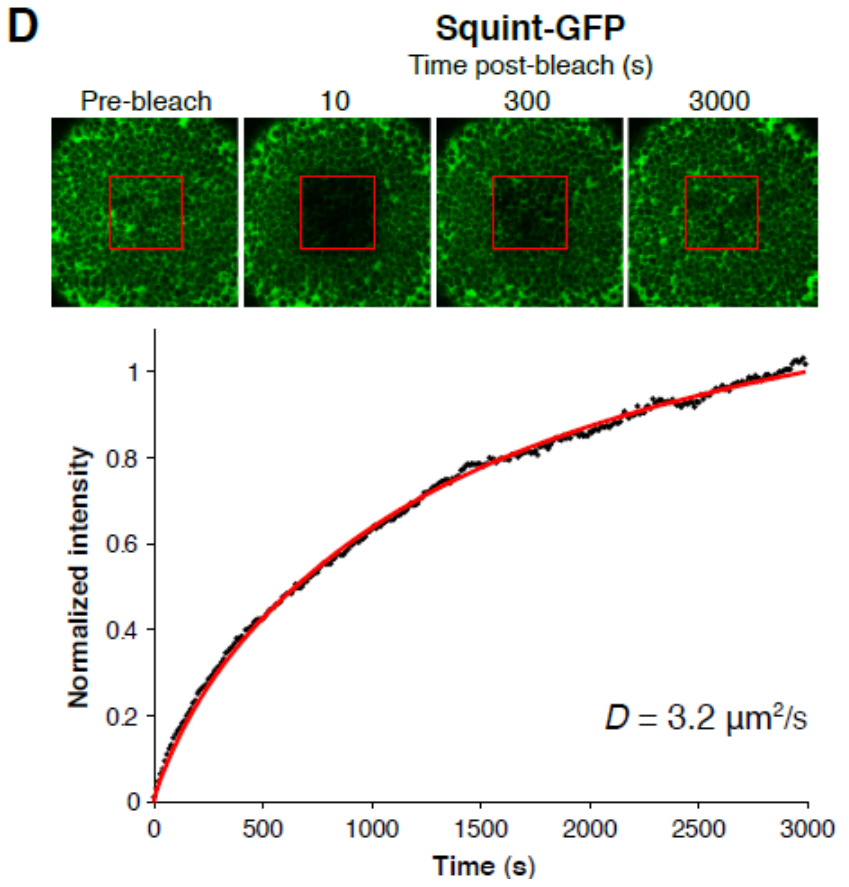

Test III: diffusion coefficient in vivo (cont.)

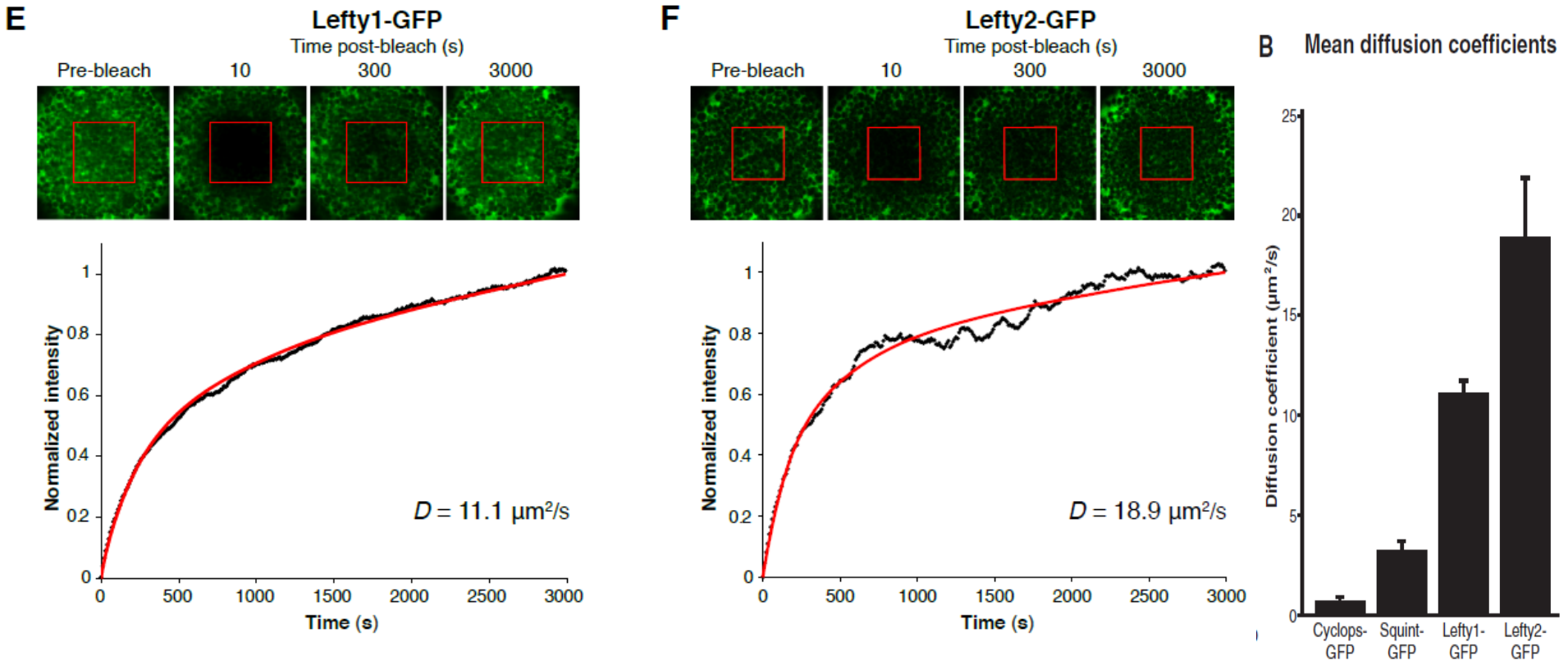

Cyclops:Squint:Lefty1:Lefty2

0.7 : 3.2 : 11.1 : 18.9

Large differences,

could explain the range difference

Validated the key point of Turing Pattern

Conclusion of this study

- Different diffusivity underlies differences in activator/inhibitor range.
- The biophysical properties (diffusion) and network structure of Nodals and Leftys support the Turing pattern of embryogenesis.
- The origin of different diffusivity remains undetermined. *Effective diffusion, not exactly pure diffusion,*

Study 2:
Quantitative genetic dosage and wavelength:
quantitative perturbation experiments and quantitative analysis

Science
AAAS

***Hox* Genes Regulate Digit Patterning by Controlling the Wavelength of a Turing-Type Mechanism**
Rushikesh Sheth *et al.*
Science **338**, 1476 (2012);
DOI: 10.1126/science.1226804

Digit patterning: Morphogen gradient or Turing pattern

- Previous consenses:for Morphogen gradient
  - Sonic Hedgehog (SHH)
  - SHH inhibits Gli3
  - SHH and Gli3 opposite gradient
  - Gli3:genetic cause of multiple digits

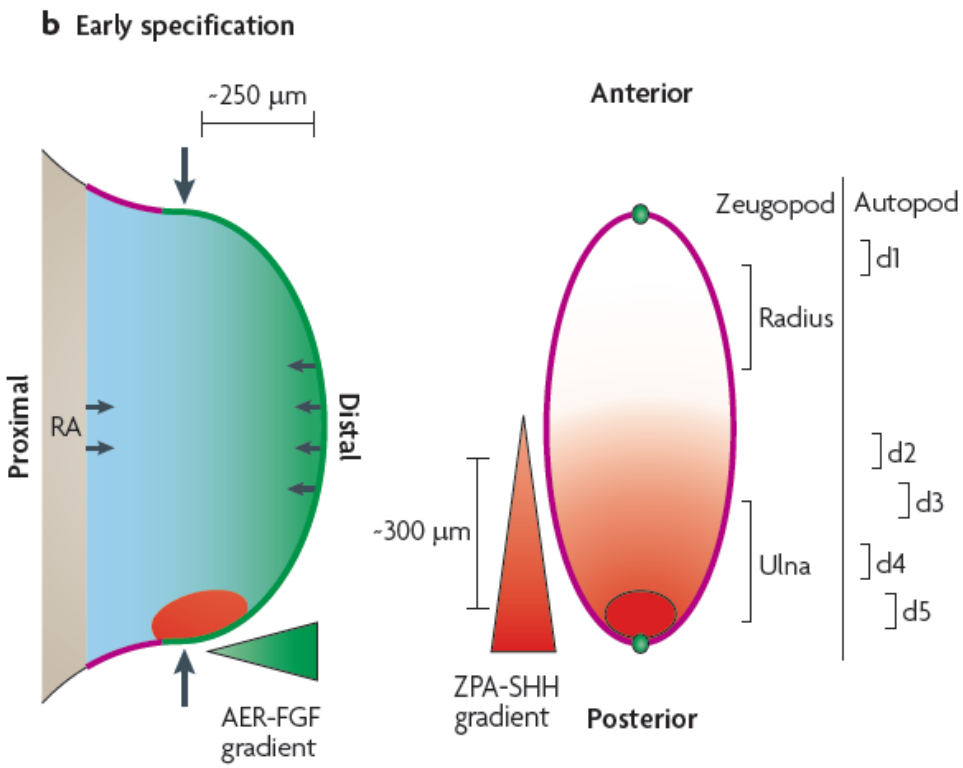

Limb bud

Digit patterning: Morphogen gradient or Turing pattern

- Evidences for Turing Pattern:
  - Mouse Gli3 and SHH:Gli3 null mutants:Identical phenotype of more digits

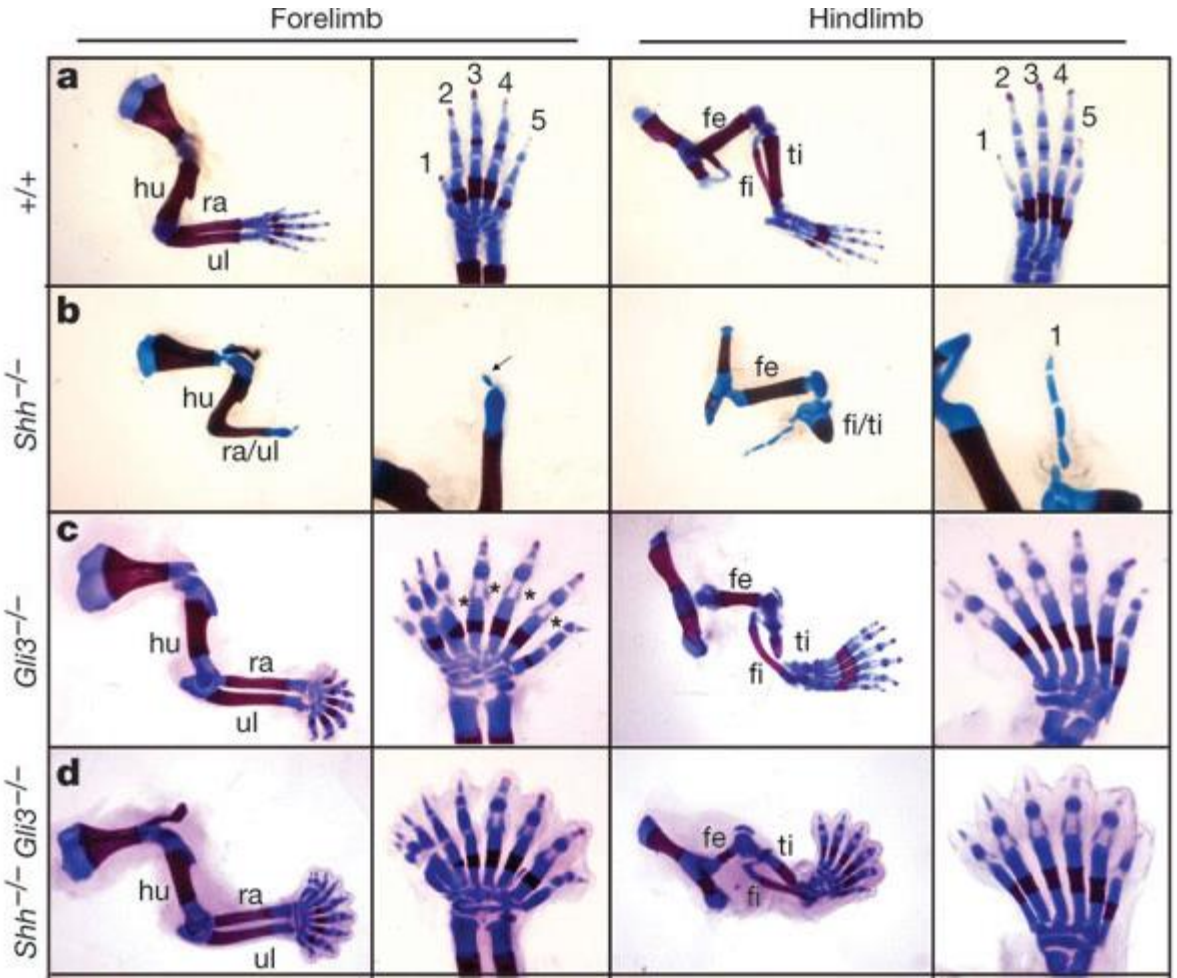

Hoxa13 suppresses digit number and digit bifurcation under Gli3-null genetic background

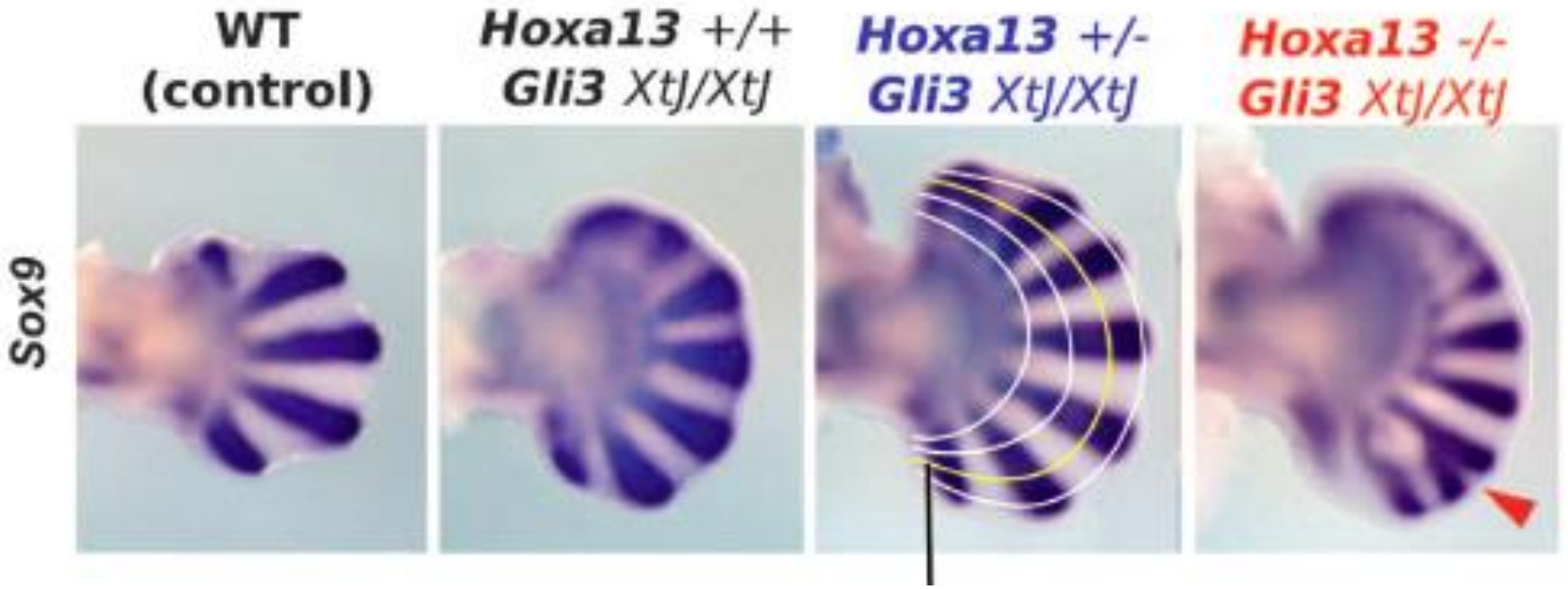

Gradually decrease Hoxa13 gradually increase digit number and delay digit formation

Quantitative assess the digit pattern

From Sox9 staining, AP length and the period (wavelength) of each digit can be quantified.

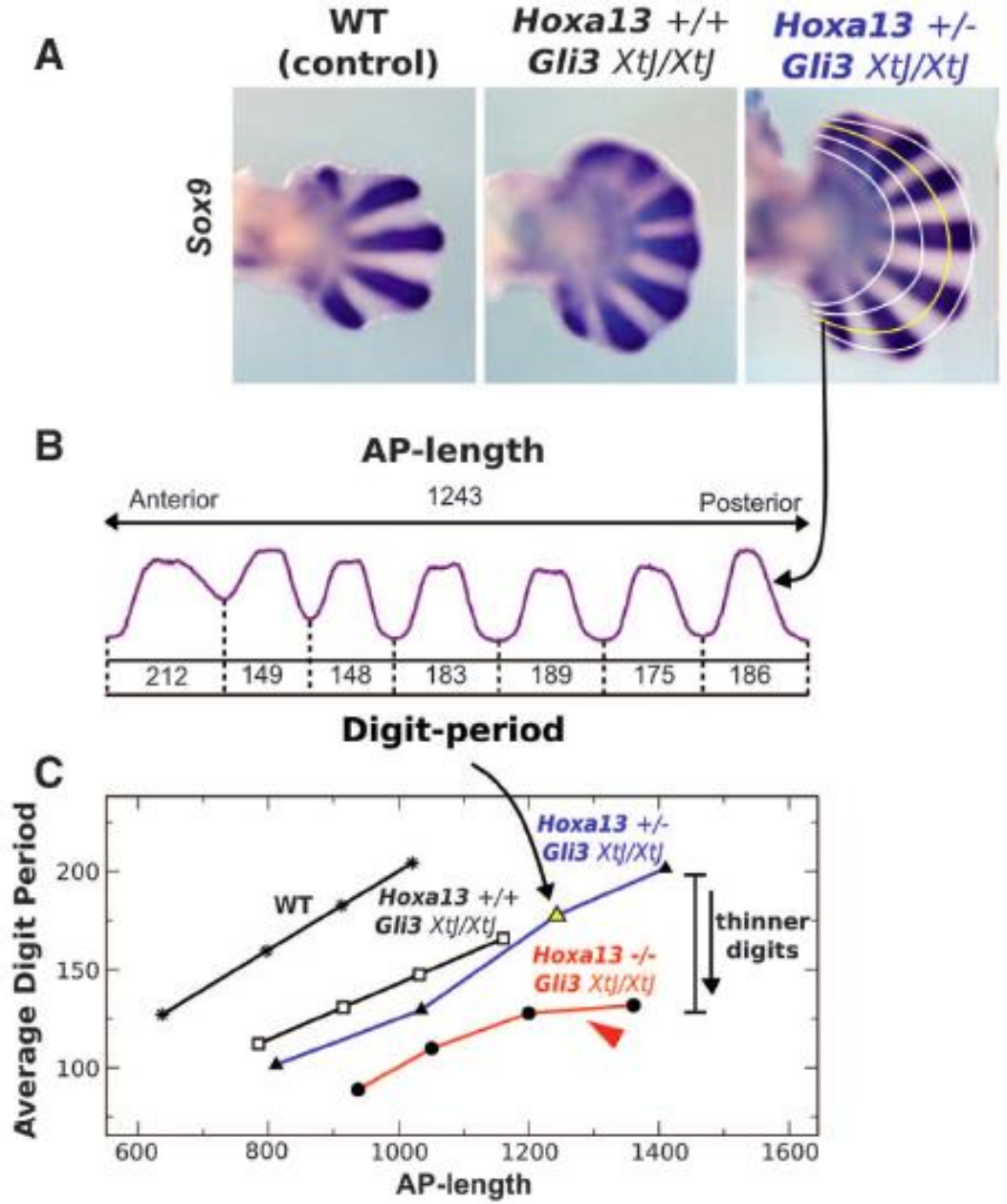

Modeling digit patterning under Gli3-null using Turing's mode

- Mathematic evidences of Turning pattern
  - Increasing development field: more digits
  - Progressice allele removal of distal Hox gene induces the formation of an increase number of thinner digit within the same space
  - Distal digit bifurcation occur

Mathematic equations

$$\frac{\partial u}{\partial t} = f(u,v) + d_u \nabla^2 u$$
$$\frac{\partial v}{\partial t} = g(u,v) + d_v \nabla^2 v$$

$$f(u,v) = f_u u + f_v v - u^3$$
$$g(u,v) = g_u u + g_v v$$

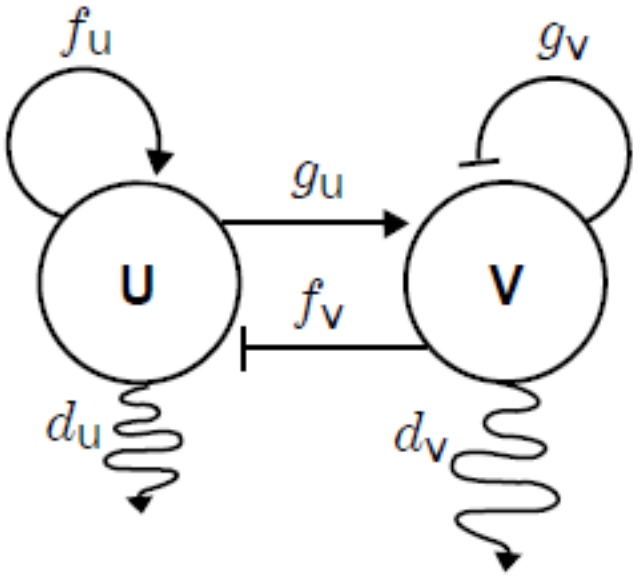

Figure S7: The network of the Activator-Inhibitor model

f_u	f_v	g_u	g_v	d_u	d_v
0.49	-0.5	0.5	-0.5	70	875

Table ST1: The parameter set used, the spatial unit is μm

Wavelength and formation rate

(not required to understand)

$$k^2 = \frac{-d_u d_v (f_u - g_v) + (d_u + d_v)\sqrt{-d_u d_v f_v g_u}}{d_u d_v (d_v - d_u)}$$

wavelength $$\omega = \frac{2\pi}{\sqrt{k^2}}$$

Speed of appearance $$\lambda_{max} = \frac{d_v f_u - d_u g_v - 2\sqrt{-d_u d_v f_v g_u}}{d_v - d_u}$$

To fit Figure 1, the only good candidate for being under the effect of Hox gene is d_v.

Wavelength quantification of the WT

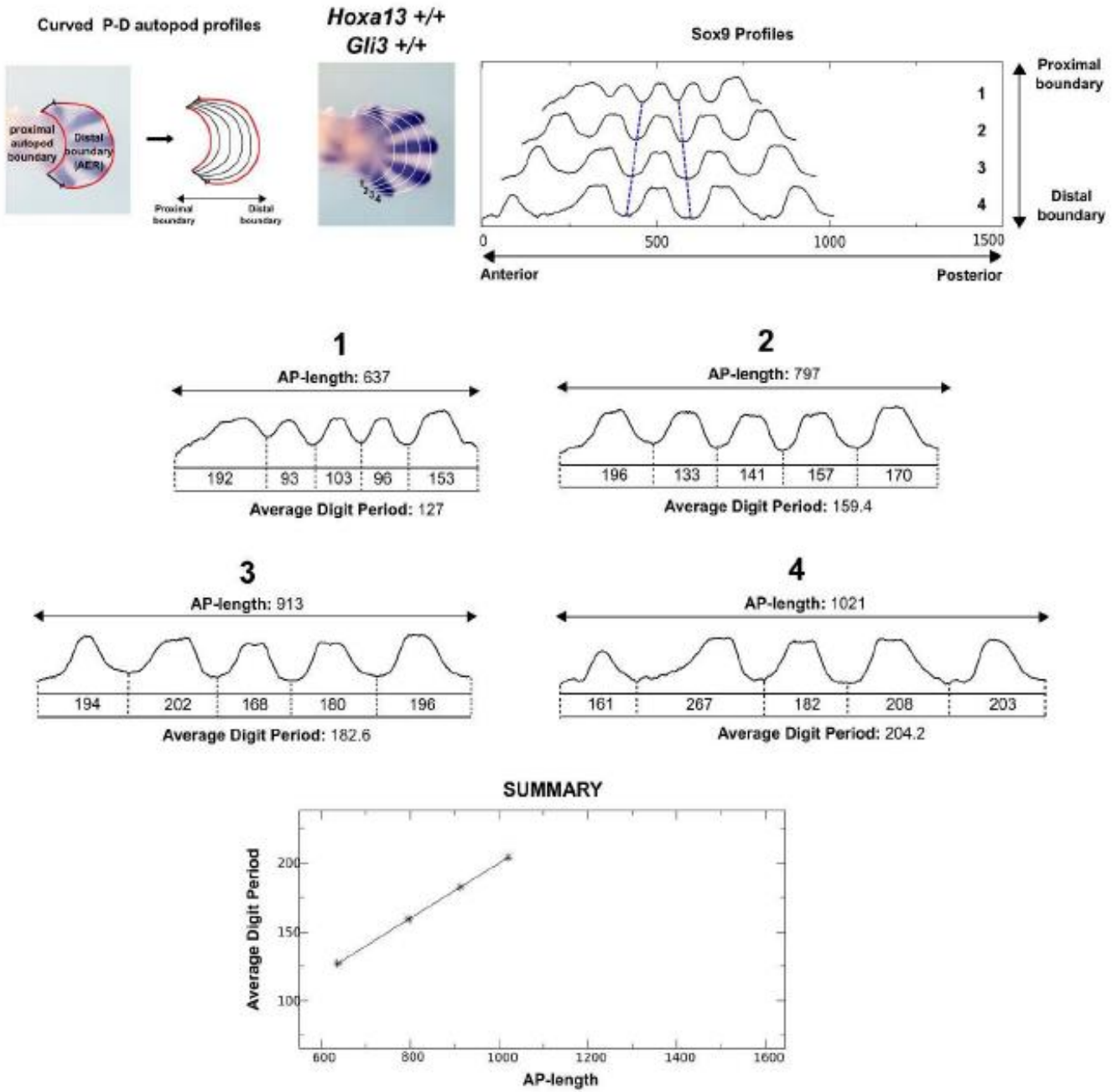

Wavelength quantification of the *Gli3 -/- ; Hoxa13 +/+* mutant

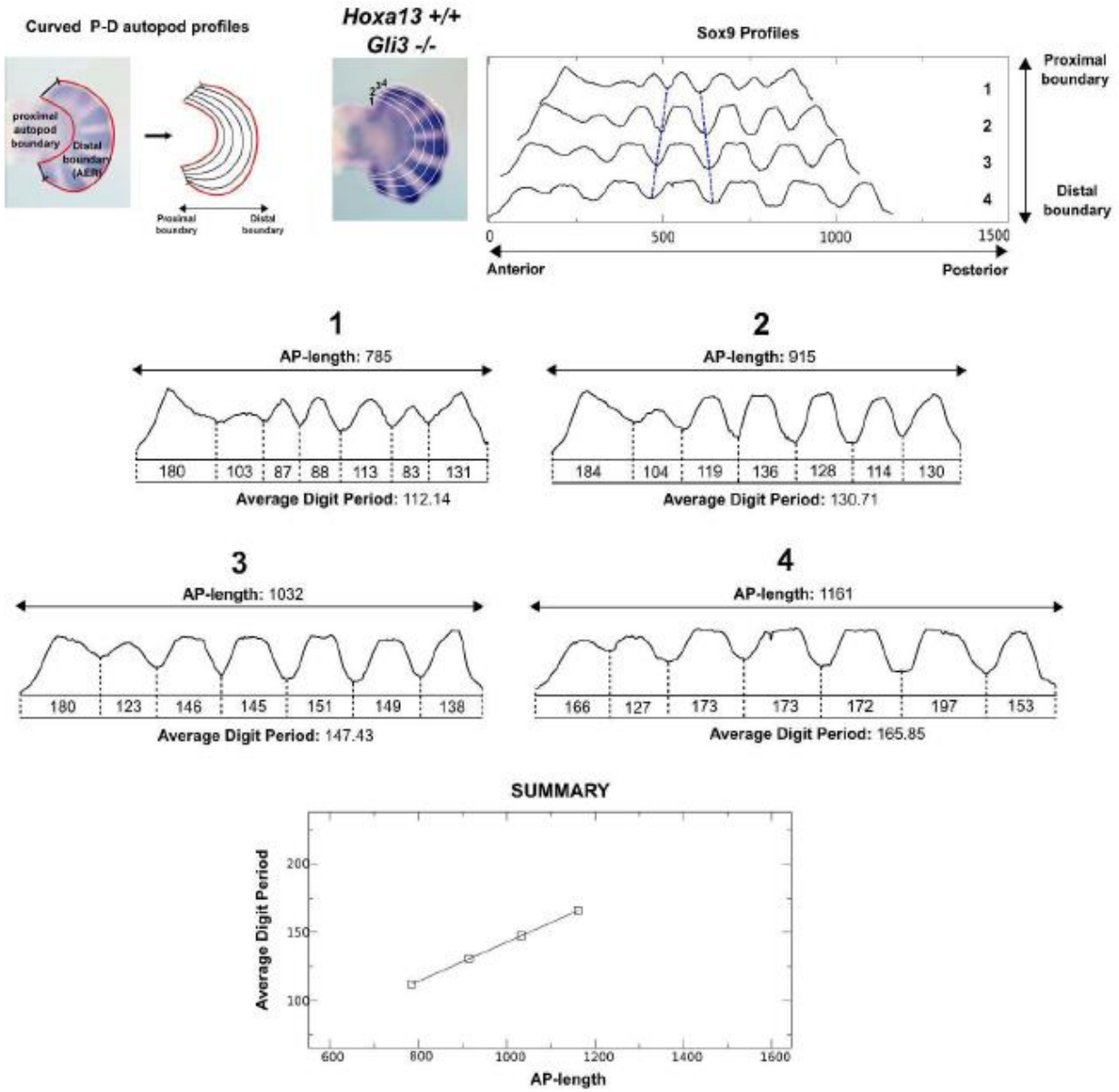

Wavelength quantification of the *Gli3 -/- ; Hoxa13 +/-* mutant

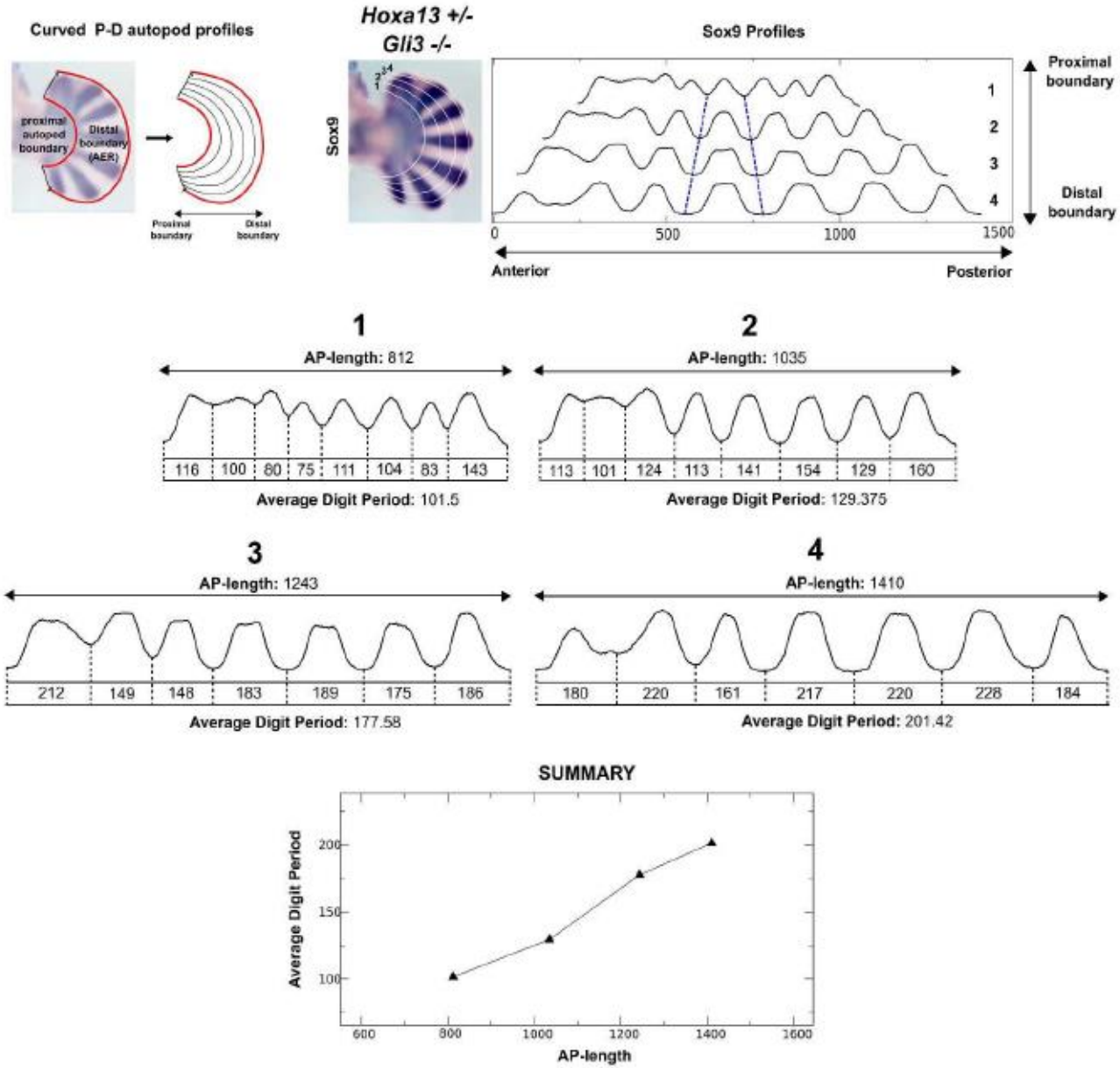

Wavelength quantification of the *Gli3 -/- ; Hoxa13 -/-* mutant

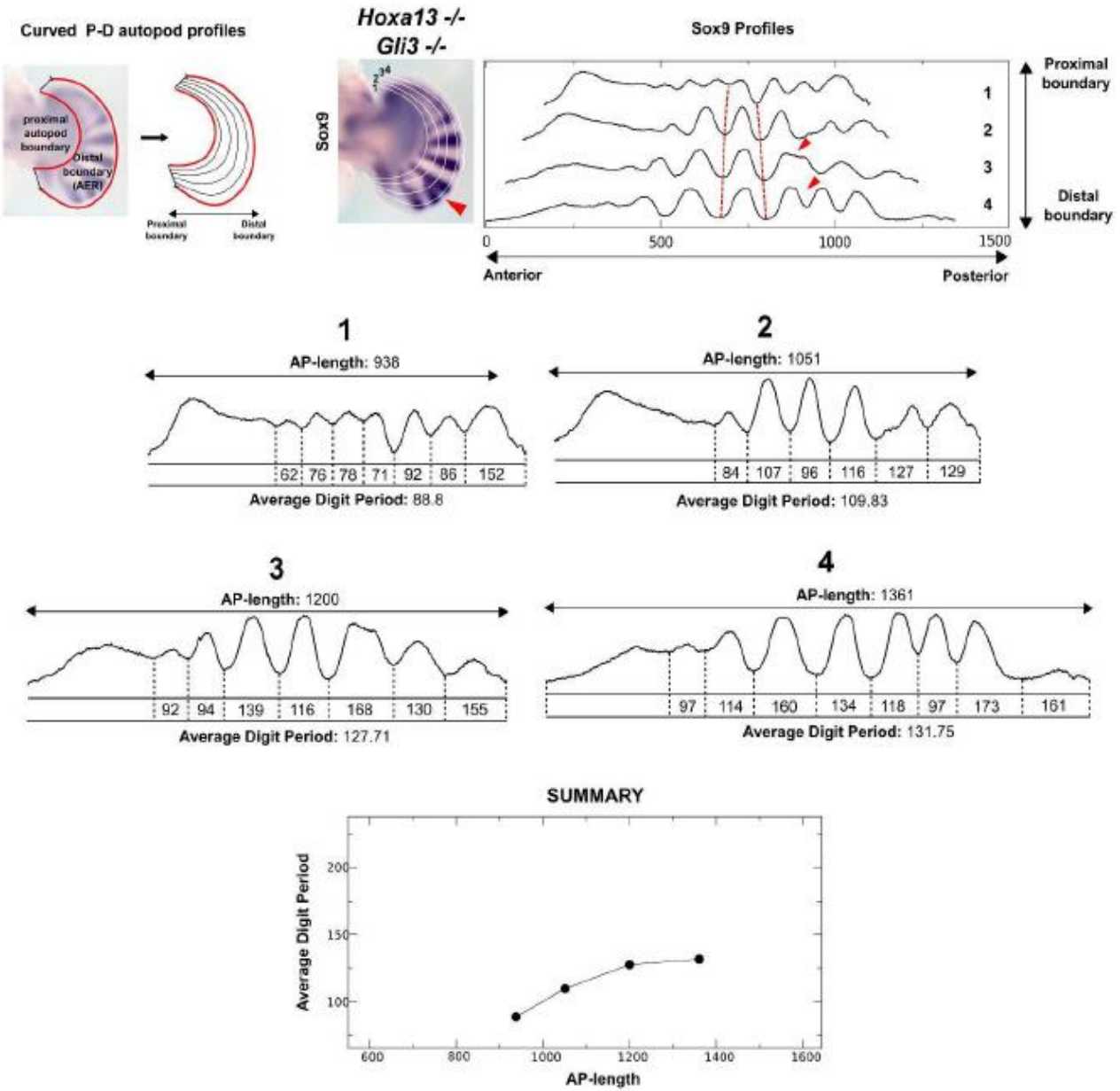

The simulation: the stripes

- $-u^3$ induces saturation effect of activator, produce stripes (matlab examples from last week).

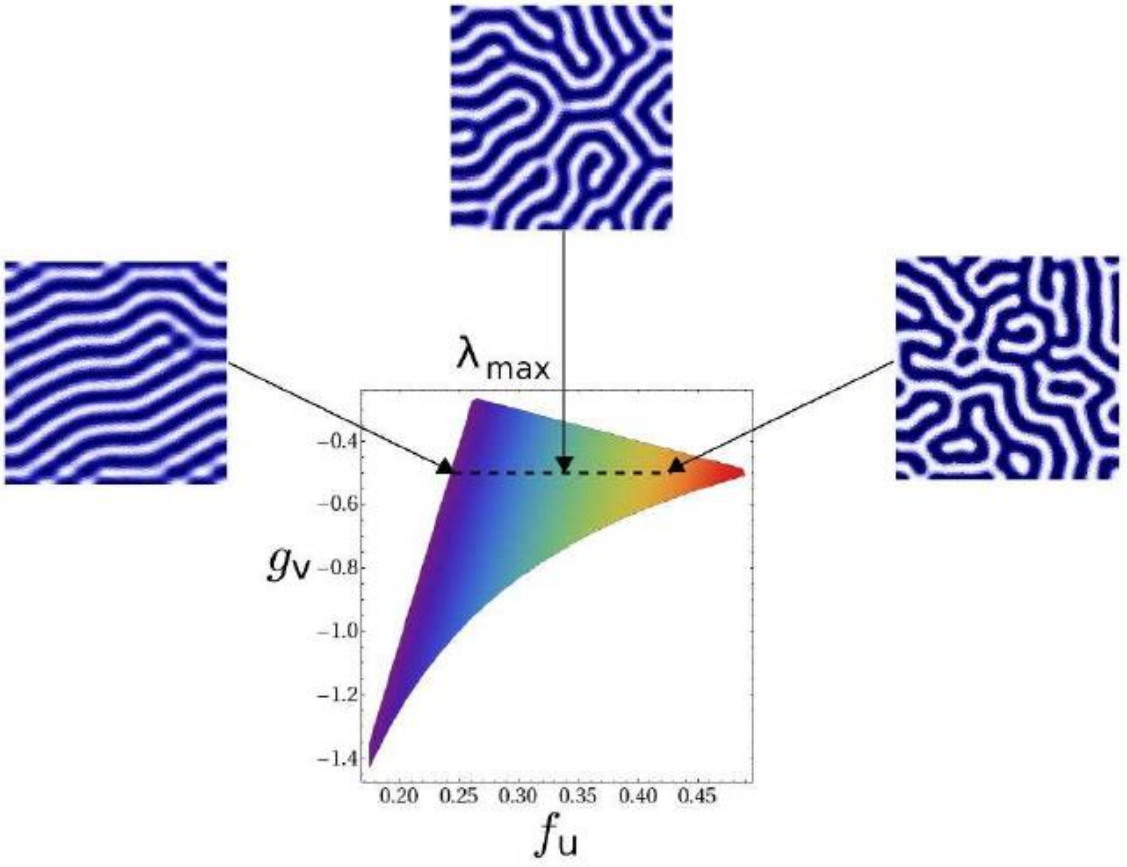

Figure S11: The effect of λ_{max} on stripe directionality

Simulation: stripe orientation

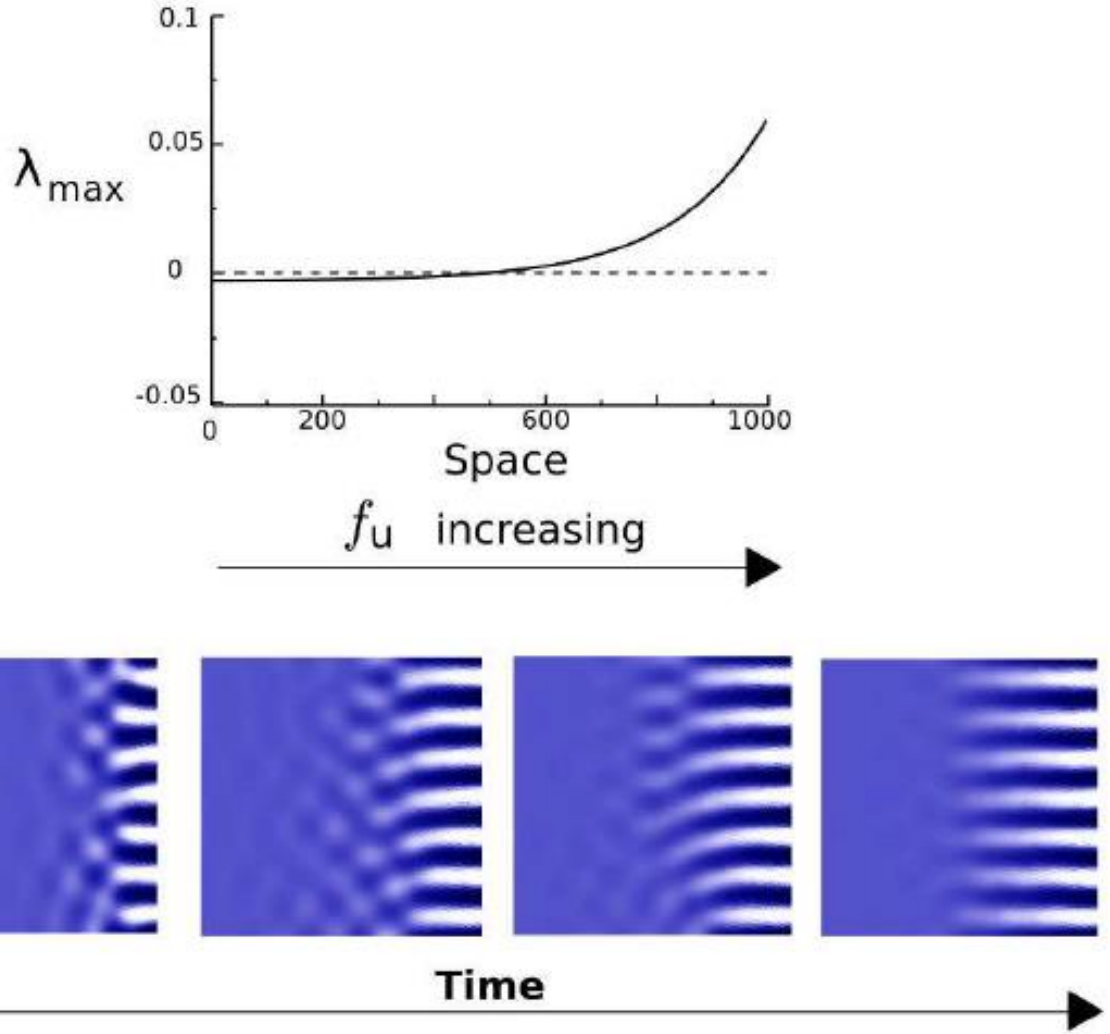

Figure S12: Stripe orientation with f_u spatial scaling

Mapping experimental distribution to model simulation

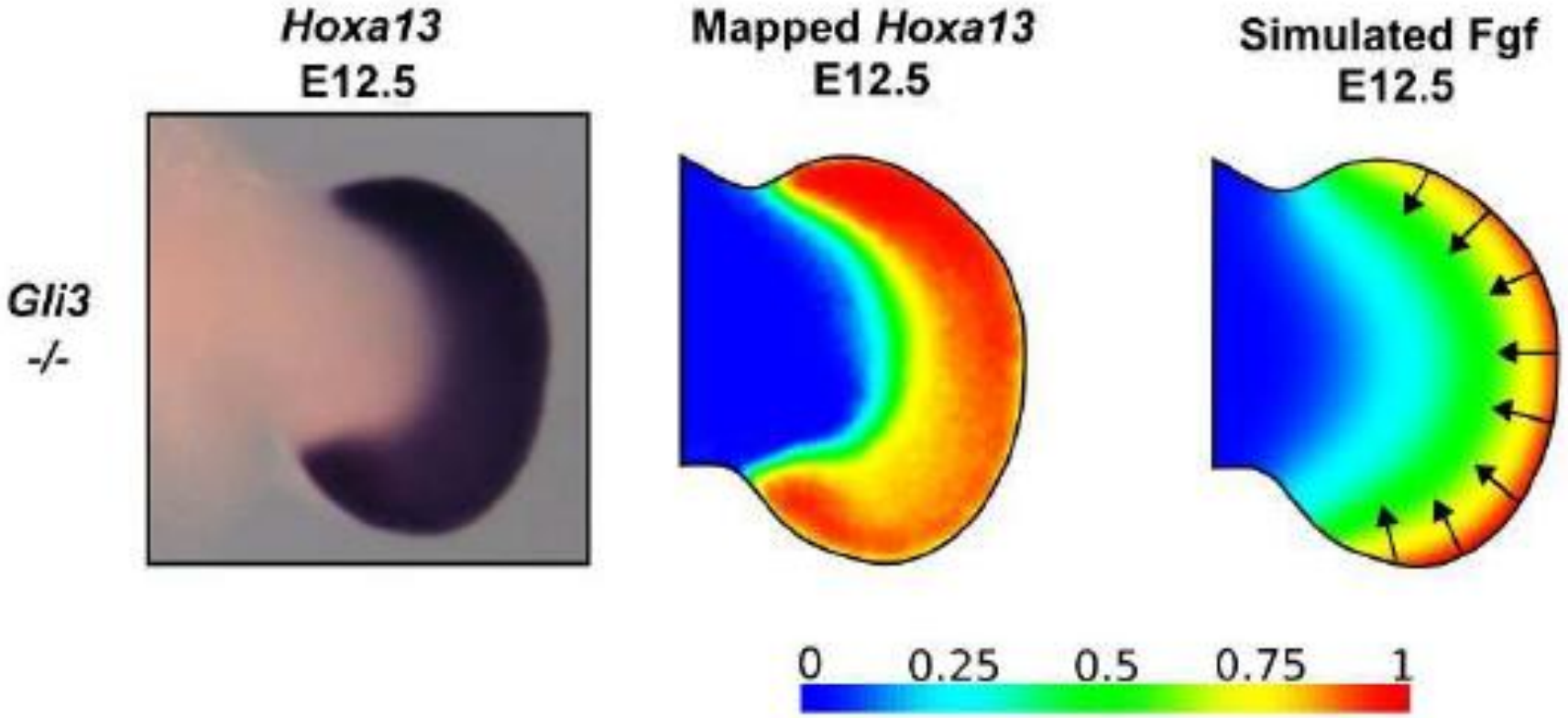

Figure S14: The patterns of *Hox* expression and Fgf signaling

Simulations for Figure 1D

D

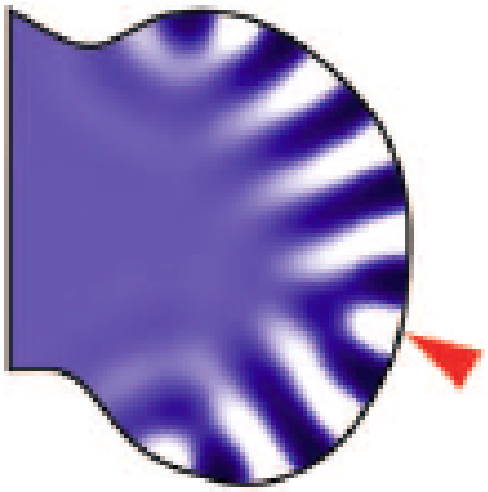

Uniform wavelength modulate f_u (FGF)

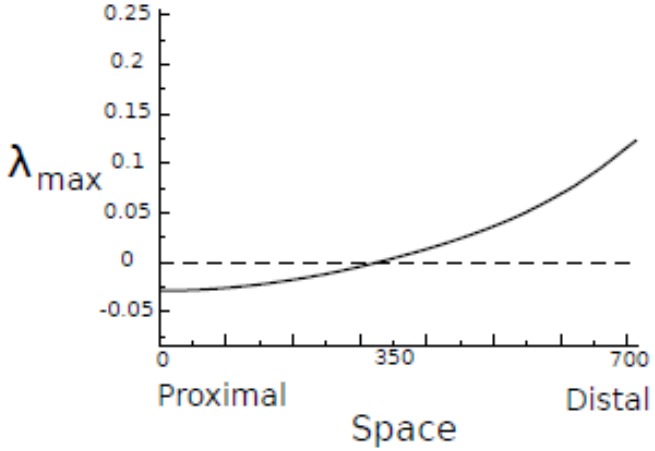

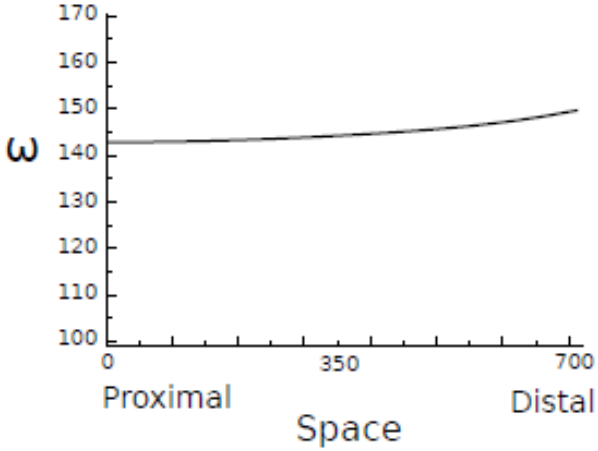

Simulations for Figure 1E

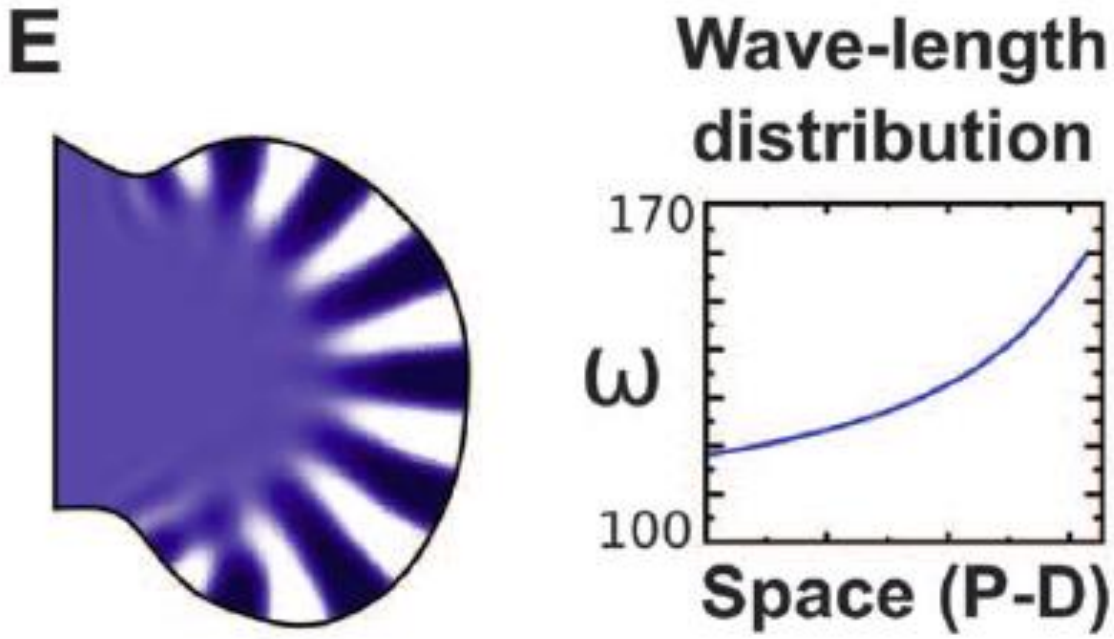

Posterior-anterior graded wavelength modulate g_u (FGF)

Gradually reducing Hoxd11-13 further increases digit number and reduces wavelength

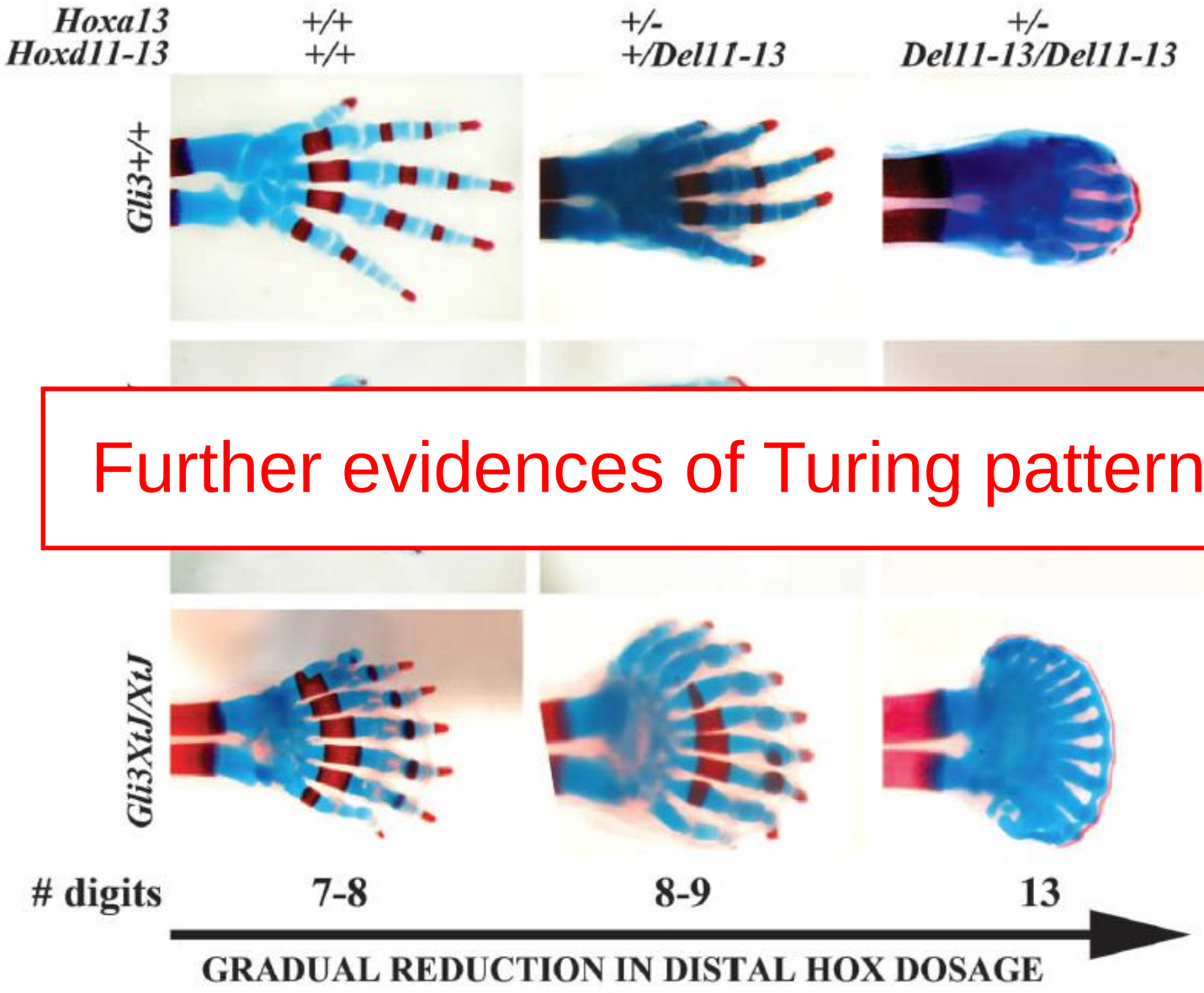

Further evidences of Turing pattern

Phenotypes of Triple mutants can be replicated by Turing model

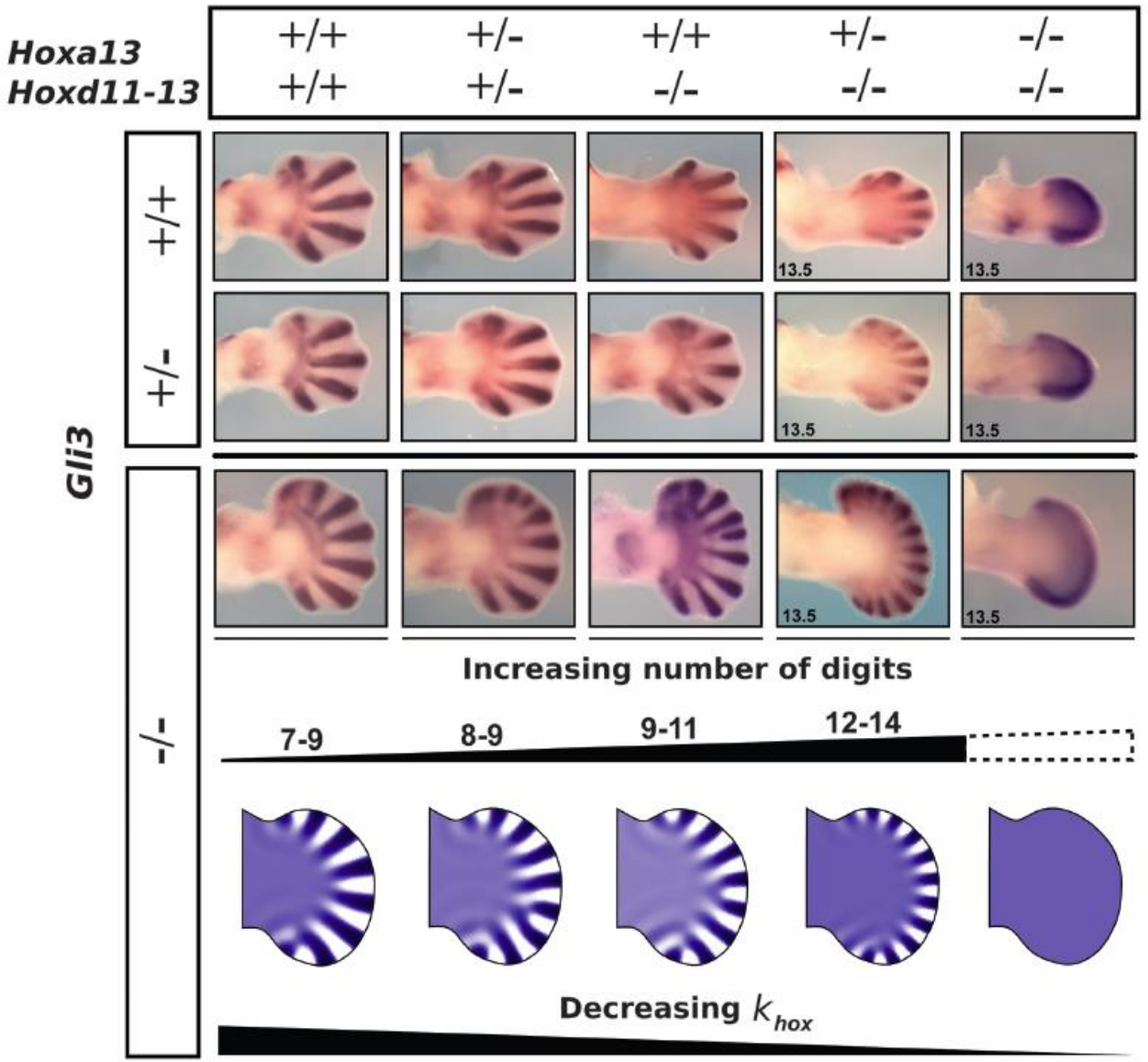

Modeling the triple mutants

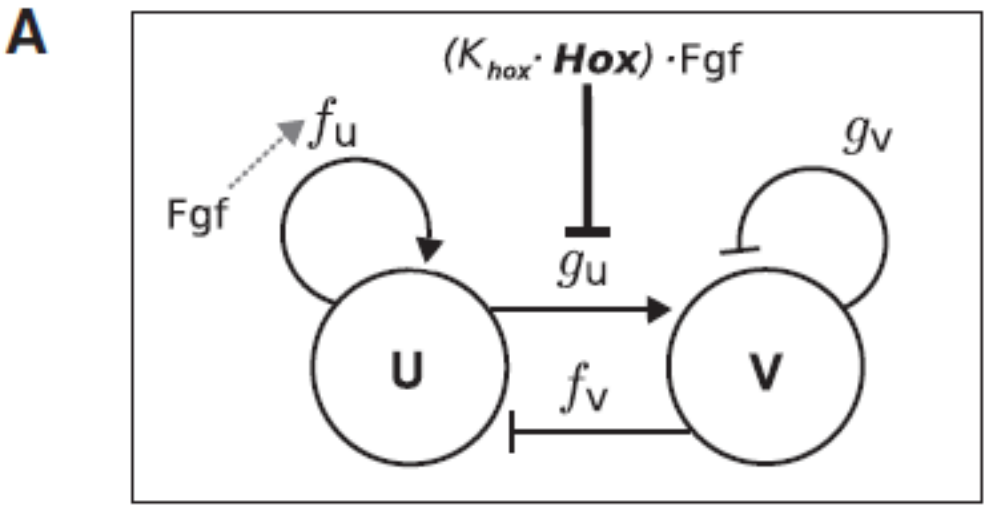

$$g(u,v) = (g_u - k_{gu} \cdot \boldsymbol{k_{hox}} Hox \cdot Fgf)u + g_v v$$

$Hoxa13$	$+/+$	$+/-$	$+/+$	$+/-$	$-/-$
$Hoxd11-13$	$+/+$	$+/-$	$-/-$	$-/-$	$-/-$
k_{hox}	1	0.7	0.5	0.2	0

Analysis of triple mutants

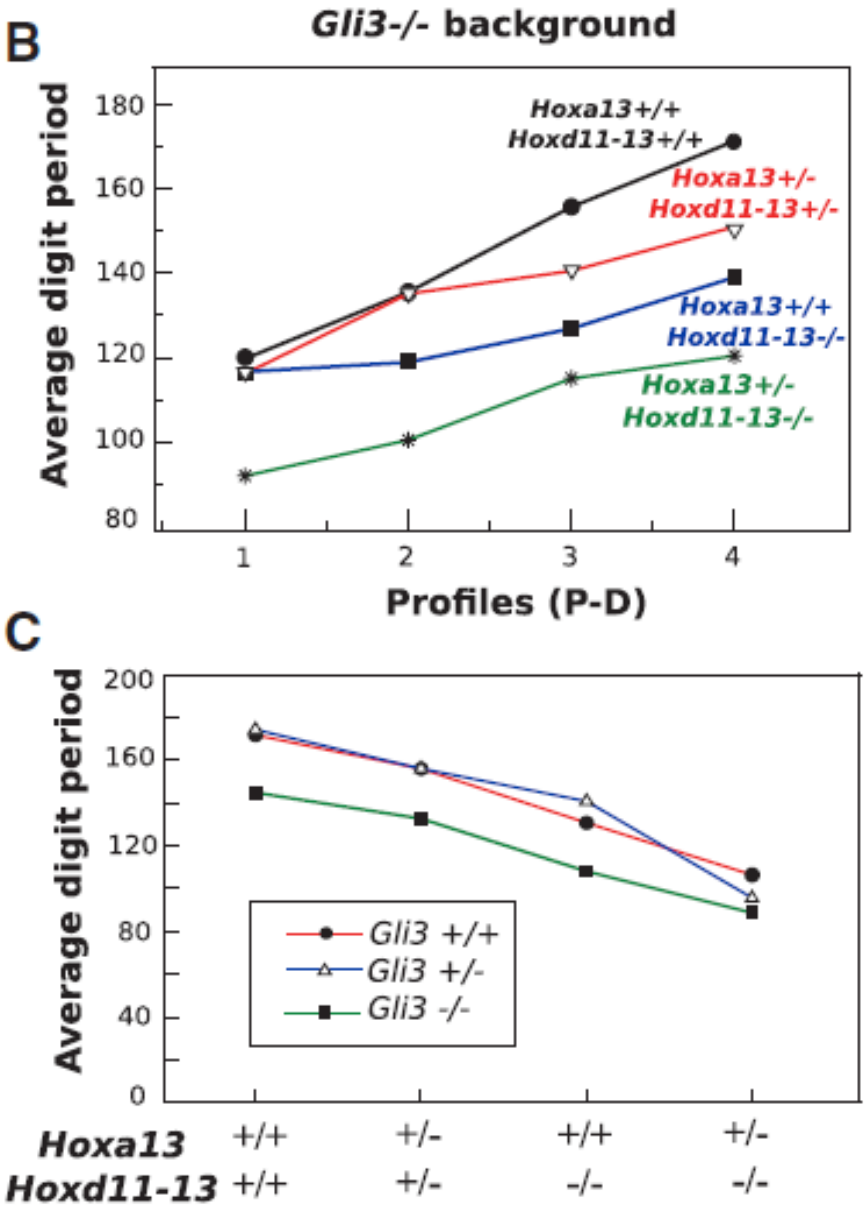

Summary of study II

- Combined genetics, quantitative experiments and modeling unveil the correlation between Hox gene dosage and the tuning of wavelength with Turing patterning of mouse digit
- Hox gene: evolutionary conserved in fin-to-limb transition.

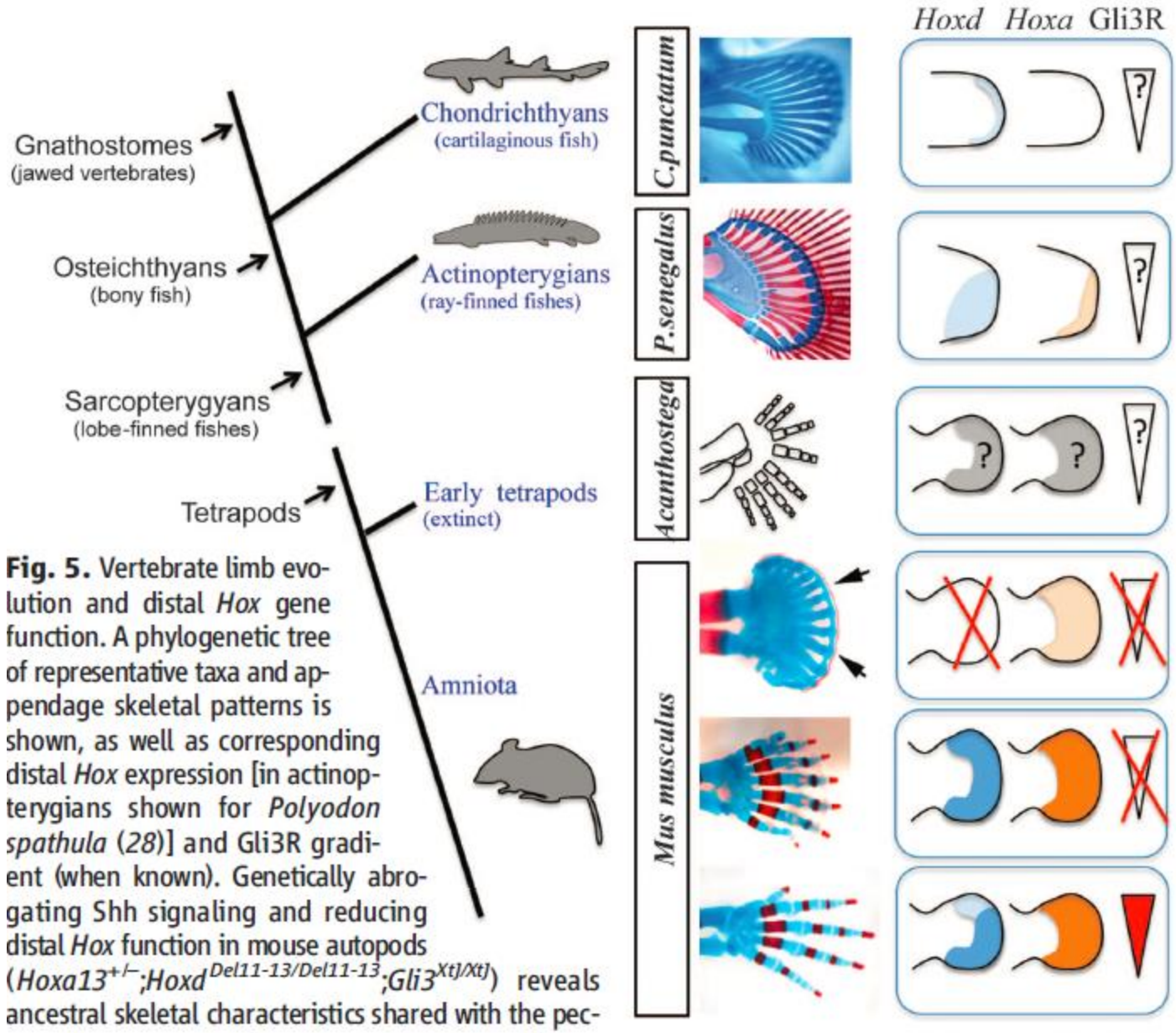

Fig. 5. Vertebrate limb evolution and distal *Hox* gene function. A phylogenetic tree of representative taxa and appendage skeletal patterns is shown, as well as corresponding distal *Hox* expression [in actinopterygians shown for *Polyodon spathula* (*28*)] and Gli3R gradient (when known). Genetically abrogating Shh signaling and reducing distal *Hox* function in mouse autopods ($Hoxa13^{+/-}$;$Hoxd^{Del11\text{-}13/Del11\text{-}13}$;$Gli3^{Xtj/Xtj}$) reveals ancestral skeletal characteristics shared with the pec-